EI 46

UDC 621.372.622:621.3.029.65:536.48

ACTA POLYTECHNICA SCANDINAVICA

ELECTRICAL ENGINEERING SERIES No. 46

Experimental studies on cooled millimeter wave mixers

ANTTI V. RÄISÄNEN

Helsinki University of Technology, Radio Laboratory
SF-02150 ESPOO 15, Finland

Thesis for the degree of Doctor of Technology accepted by the Helsinki University of Technology, Otaniemi.

HELSINKI 1980

ISBN 951–666–127–0
ISSN 0001–6845

VTT OFFSETPAINO 1980
674/6

PREFACE

The research work for this dissertation was carried out during 1975–1980, while I worked as a research assistant for the Academy of Finland.

During 1975–1978 and 1980 I worked at the Radio Laboratory of the Helsinki University of Technology. I wish to thank Professor Martti Tiuri, the director of the Radio Laboratory, for providing me with the opportunity to do this work and also for many valuable discussions. I am grateful also to Dr. Pekka Somervuo, Dr. David Meharry and Juhani Peltonen from the Radio Laboratory for their kind help.

During 1978–1980 I worked at the Five College Radio Astronomy Observatory of the University of Massachusetts. I would like to express my gratitude to Professor Richard Huguenin, the director of the FCRAO, for providing me with the opportunity to work for the observatory. I wish to give my sincere thanks to Assistant Professor Peter Parrish, Assistant Professor Paul Goldsmith, Dr. Read Predmore, Jose Marrero, Richard Kot and Michael Brewer, whose co-operation during 1978–1980 was invaluable. I am also obliged to Professor Sigfrid Yngvesson, Dr. Neal Erickson and Dr. Gerhard Sollner for their encouragement and help.

Finally, I am deeply indebted to my wife, Hannele, for her patience and support over the years.

This research work was partially financed by the Emil Aaltonen Foundation, the Finnish Cultural Fund, the Walter Ahlström Foundation, the Leo and Regina Wainstein Foundation, the ASLA-Fulbright Foundation, the National Science Foundation (the United States), the Foundation for the Promotion of Technology and the Magnus Ehrnrooth Foundation.

Helsinki, October 2, 1980

Antti V. Räisänen

ABSTRACT

The design and performance of two cooled mm-wave mixers is described. A Josephson point contact mixer was designed for 30–40 GHz. The Nb point contact is located in a symmetrical Nb waveguide flange using suitable insulating material. This construction allows the junction to be adjusted at T_{room} and makes it mechanically stable against shocks and temperature cycling. At 36 GHz the conversion loss was measured to be 5 dB when using an IF of 60 MHz. The mixer works evenly at frequencies 30–40 GHz. A cooled Schottky diode mixer was designed for 75–120 GHz. New details of this mixer include improved waveguide, backshort, RF filter and IF matching and bias circuit designs. This mixer is used in a cooled receiver (15 K) where LO is coupled by an adjustable ring-filter. The mixer is followed by a 4.5–5.0 GHz IF system of T_{IF} = 24 K. For this receiver DSB noise temperatures of T_{RDSB} = 140–230 K have been measured at any LO frequency from 75 to 120 GHz. The best SSB receiver noise temperature measured is T_{RSSB} = 275 K at 88 GHz including a quasi-optical feed system. This implies a mixer noise temperature of $T_{MSSB} < 100$ K. Finally a discussion on noise temperature and noise figure calculations and noise measurements is presented.

CONTENTS

LIST OF SYMBOLS

B	bandwidth
C_j, C_{j0}	capacitance of Schottky barrier
C_{ch}	capacitance of RF filter
C_F	fringing capacitance
C_n, C_N	capacitances in equivalent circuits
e	charge of electron
E_0	potential energy parameter of Schottky I-V-curve
f_c	cut-off frequency
f_i	image frequency
f_s	signal frequency
f_{IF}	intermediate frequency
f_{LO}	local oscillator frequency
f_0	Josephson frequency
F	noise figure
F_M, F_{MDSB}, F_{MSSB}	mixer noise figure
$g(t)$	conductance
g_n	conductance parameter
G	available power gain
G_j	conductance of Schottky barrier
G_C	conversion gain
G_{IF}	IF amplifier gain
h	Planck's constant
$\hbar = h/2\pi$	modified Planck's constant
i_{RF}	RF current
$I, I(t)$	current
I_c	critical current of Josephson junction
I_s	amplitude of signal current
I_{BIAS}, I_{DC}	bias current
I_{LO}	amplitude of LO current
I_0	height of the 0th step in Josephson I-V-curve
I_{00}	saturation current of Schottky barrier
k	Boltzmann's constant
l_n, L_n, L_N	inductances in equivalent circuits
L, L_C	conversion loss
L_{ch}	inductance of RF filter
L_i	image conversion loss
L_p	loss due to parasitics of Schottky diode
L_s	signal conversion loss
L_{DSB}	DSB conversion loss
L_F	loss due to ring-filter and feed horn
m^*	electron effective mass
N_{in}	input noise power

N_{int}	intrinsic noise power
N_{out}	output noise power
N_C, $N_{C,IF}$	output noise power for cold input
N_D	doping density of semiconductor
N_H, $N_{H,IF}$	output noise power for hot input
P_{LO}	LO power
R	normal resistance of Josephson junction
R_d	diode resistance
R_{dyn}	dynamic resistance of Josephson junction
R_j	resistance of Schottky barrier
R_s	series resistance of Schottky diode
t, t'	time
T	ambient temperature
T_e	equivalent noise temperature
T_i	image load temperature
T_{int}	intrinsic noise temperature
T_{room}	room temperature
T_s	signal load temperature
T_{sys}	system noise temperature
T_A	antenna noise temperature
T_C	temperature of cold reference load
T_D	diode noise temperature
T_H	temperature of hot reference load
T_{IF}	IF amplifier noise temperature
T_M, T_{MDSB}, T_{MSSB}	mixer noise temperature
T_R, T_{RDSB}, T_{RSSB}	receiver noise temperature
T_0	absolute reference noise temperature, 290 K
V, $V(t)$	voltage
V_j	voltage across Schottky barrier
V_s	amplitude of signal voltage
V_{DC}	bias voltage
V_{LO}	amplitude of LO voltage
V_0	potential parameter of Schottky I-V-curve
X_L	inductive series reactance of Josephson junction
X_n	reactance
Y	ratio in noise measurements (Y-factor)
Z_0	generator impedance
Z_n, Z_N	characteristic impedances
ϵ_r	relative dielectric constant
ϵ_0	dielectric constant of vacuum
η	ideality factor of Schottky diode
θ_n	electrical length of transmission line
λ	wavelength
λ_g	wavelength in waveguide
ρ	resistivity
τ	optical depth
ϕ, $\phi(t)$	phase angle
ϕ_0	integration constant
ω_s	angular signal frequency

ω_{IF}	angular intermediate frequency
ω_{LO}	angular LO frequency
ω_{RF}	angular radio frequency
ω_0	angular Josephson frequency
Ω	normalized frequency of Josephson junction

AC	alternating current
DC	direct current
IF	intermediate frequency
LO	local oscillator
RF	radio frequency
DSB	double sideband
LSB	lower sideband
SSB	single sideband
USB	upper sideband
VSWR	voltage standing wave ratio

1. INTRODUCTION

The portion of the electromagnetic radiation spectrum having frequencies between 30 and 300 GHz is called millimeter waves. During the last few years these frequencies have become very important in communications, electromagnetic metrology, remote sensing and especially in radioastronomy. In all these applications the measurements are receiver noise limited, because the lack of millimeter wave amplifier forces the first stage of the receiver to be a mixer. As thermal noise plays an important role in the noise performance of mixers, cooling is a natural way to reduce the noise and, thus, improve the sensitivity.

Since WEINREB's and KERR's work in 1973 [42] there has been considerable effort to develop cooled millimeter wave receivers. These receivers utilize resistive Schottky diodes, Josephson point contacts, superconductor-insulator-superconductor (SIS) junctions, Schottky varactors or InSb bolometers as mixing elements.

The resistive Schottky diode is by far the most common type of mixing element. Its operation is quite well understood and the technology to produce GaAs diodes is very advanced. Thus, reliable cooled mixers have been built up to frequencies of 170 GHz. So far, the best receivers utilizing a Schottky diode are KOLLBERG's receiver at Onsala Space Observatory having T_{RSSB} = 240 K at f_s = 85 GHz [17] and LINKE's receiver at Bell Laboratories having T_{RSSB} = 300 K at f_s = 115 GHz [19].

The Josephson point contact mixers have been intensively investigated in research laboratories but no receivers have come to the stage of »field use». The best mixer results are T_{MSSB} = 120 K and L_C = 0 dB at f_s = 115 GHz [38] and T_{MSSB} = 54 K and conversion gain G_C = 1.3 dB at 36 GHz [37], but one should notice that in both of these experiments the total receiver noise temperature was thousands of Kelvins because of the cold attenuators used in front of the mixer to prevent room temperature noise from saturating the junction.

A new, more promising superconducting mixing element is the SIS junction. A new technology has been developed at IBM and Bell Laboratories to produce reliable junctions. The theory of this device promises high conversion gain and quantum limited noise temperature [36]. In the laboratory this performance has laready been achieved [30]. By now only one receiver of this type has been built and successfully used at the telescope. This receiver was developed at Bell Laboratories and is being used at Owens Valley Radio Observatory. For this receiver a SSB receiver noise temperature of 230 K at f_s = 115 GHz has been measured [5]. The mixing element is a Pb-In-Bi junction.

Cooled mixers of minor importance are the Schottky varactor down converter and the InSb bolometer mixer. For the former a mixer noise temperature T_{MSSB} = 150 K and L_C = 11.5 dB were measured when used as an upper sideband down converter at 115 GHz [41]. The device is, however, very unreliable. The latter, the InSb bolometer mixer, is also a low noise mixer leading to T_{RDSB} = 250 K at f_{LO} = 115 GHz [27], but its very narrow IF bandwidth (< 4 MHz) limits the use.

When the Radio Laboratory of the Helsinki University got a new mm-wave telescope in 1974, the interest in cooled receivers for radioastronomical observations arose also here. As it is well known, cooled receivers are not commercially available. Therefore every observatory has to build receivers of its own. Because no ultimate limits have been reached anywhere in the development of cooled mixers, it is reasonable, not to

copy directly the reported designs but to develop them further. This report is part of such development work.

In this work the design and performance of two cooled millimeter wave mixers is described. One uses a Josephson point contact and the other a Schottky diode as a mixing element. The Josephson point contact mixer was designed for frequencies 30–40 GHz and the cooled Schottky diode mixer for frequencies 75–120 GHz. Before the description of the experimental work a short review of the theory is presented in each case.

The main emphasis of this work is clearly on experiment. However, in the appendix a longer discussion on the noise temperature and noise figure formulas is presented. In this discussion the approach is philosophical; its purpose is to try to unify the use of noise formulas and not at all to discuss on the origin of the noise.

2. JOSEPHSON POINT CONTACT MIXER

2.1. Theory of operation

The Josephson effects arise [12] when two pieces of superconductor are weakly coupled, i.e. separated by some sort of barrier. The barrier can, for example, be a thin insulating film (e.g. an oxide layer), a normal metal film, or a superconductor of lower critical current than the superconductor on each side.

The current $I(t)$ and voltage $V(t)$ of an ideal Josephson junction follow the equations [13]:

$$I(t) = I_c \sin\phi(t) \tag{1}$$

and

$$\frac{d\phi(t)}{dt} = \frac{2eV(t)}{\hbar}, \tag{2}$$

where I_c is the critical current of the junction, which depends on the junction structure, material, and temperature; $\phi(t)$ is the phase difference between the wave functions describing the superconducting state on each side of the junction; e is the charge of an electron; and $\hbar$ is Planck's constant h divided by 2π.

When these equations are combined, the following expression for the current is obtained

$$I(t) = I_c \sin\left[\frac{2e}{\hbar}\int_0^t V(t')dt'\right], \tag{3}$$

revealing the usefulness of the Josephson junction as a mixer. Equation (3) shows that a constant voltage V_{DC} applied to the junction causes an alternating current to flow at the Josephson frequency

$$f_0 = \frac{2e}{\hbar} V_{DC} = 483.6\ \text{MHz}/\mu\text{V}. \tag{4}$$

This means that the Josephson junction is an active element which can convert DC power into AC and vice versa.

The most common type of Josephson junction in millimeter wave mixers is the point contact junction. A point contact consists of a piece of superconductor with a sharply pointed end being pressed against a flat surface of another piece of superconductor. The advantages of a junction of this type are its low contact capacitance and high contact resistance.

The properties mentioned above lead to an equivalent circuit of the point contact as in Figure 1, where the ideal Josephson junction is shunted by a resistor [23]. This model is commonly called the RSJ-model (resistively shunted junction model). The equation between the current and voltage can now be written

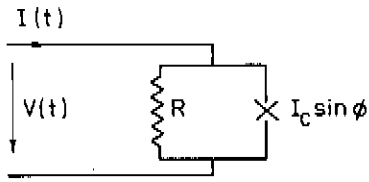

Figure 1. The RSJ-model for the Josephson point contact junction.

$$I(t) = I_c \sin\phi(t) + \frac{\hbar}{2eR}\frac{d\phi(t)}{dt} = I_c \sin\left[\frac{2e}{\hbar}\int_0^t V(t')dt'\right] + \frac{V(t)}{R}. \qquad (5)$$

This equation gives a hyperbolic form to the static I-V-characteristic when the junction is fed from a current source. In Figure 2 a typical measured I-V-characteristic is illustrated.

To understand the mixing phenomenon, a situation is considered where the voltage $V(t) = V_{DC} + V_s \cos\omega_s t + V_{LO}\cos\omega_{LO} t$ is applied to a Josephson junction. Thus, besides the bias voltage, there are alternating voltages caused by the signal source and the local oscillator. Inserting this voltage into Equation (5) and using mathematical identities, one obtains

$$I(t) = I_c \sum_{m=-\infty}^{\infty}\sum_{n=-\infty}^{\infty} (-1)^{m+n} J_m\left(\frac{2eV_s}{\hbar\omega_s}\right) J_n\left(\frac{2eV_{LO}}{\hbar\omega_{LO}}\right) \sin\left(\frac{2eV_{DC}t}{\hbar} + \phi_0 - m\omega_s t - n\omega_{LO} t\right) + \frac{V(t)}{R}, \qquad (6)$$

where $J_m(x)$ and $J_n(x)$ are Bessel functions of the first kind of integer order m and n, and ϕ_0 is a constant of integration.

It can be seen that under the given conditions oscillating supercurrents can exists in the junction at difference and sum frequencies. In addition, when $\omega_0 = (2e/\hbar)V_{DC} = m\omega_s + n\omega_{LO}$, there is a non-oscillating supercurrent term which appears as a constant voltage spike in the I-V-characteristic.

In the above analysis a RF voltage source is assumed. In a more realistic case the junction is fed from a RF current source as shown in Figure 3, but now the analysis becomes complicated. When RF power is applied to the junction constant voltage steps

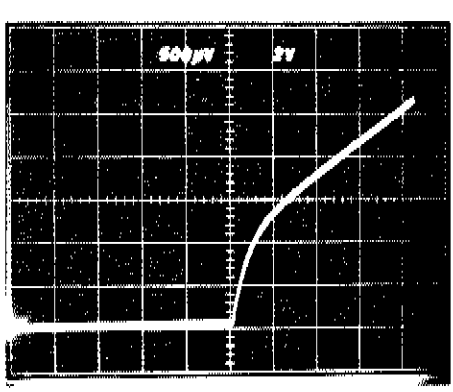

Figure 2. A typical measured I-V-curve of a point contact (junction No. 6, Table 1) fed from a current source (current on horizontal scale).

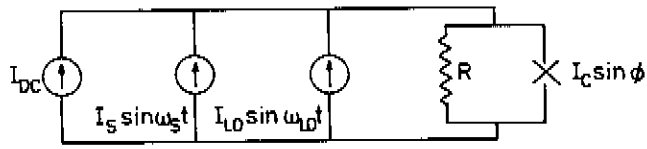

Figure 3. A point contact fed from current sources.

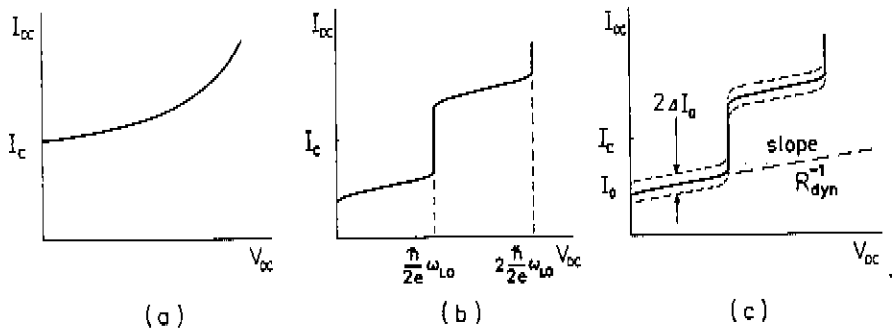

Figure 4. The effect of microwave power on the *I-V*-characteristic: a) no RF signal, b) LO signal applied, c) variation of step heights due to the modulation.

appear in the *I-V*-characteristic instead of spikes (Figure 4). The heights of these steps are determined by the incident radiating power [13].

In the situation of Figure 3 the current applied to the junction is

$$I(t) = I_{DC} + I_s \sin\omega_s t + I_{LO} \sin\omega_{LO} t$$
$$\cong I_{DC} + (I_{LO} + I_s \cos\omega_{IF} t) \sin\left(\omega_{LO} t + \frac{I_s}{I_{LO}} \sin\omega_{IF} t\right). \quad (7)$$

Here the assumptions $|\omega_{IF}| = |\omega_s - \omega_{LO}| \ll \omega_{LO} \cong \omega_s$ and $I_s \ll I_{LO}$ are made. If the slow phase modulation in the above expression is neglected, a situation is obtained where a RF current is amplitude modulated at ω_{IF} by the small signal I_s. This makes the *I-V*-characteristic move up and down at the angular frequency ω_{IF} as illustrated in Figure 4c. The IF response is now easily understood.

Expressions for the conversion loss and noise temperature of the Josephson point contact mixer are derived in Reference [37] from the basis of the current driven junction model.

2.2. Design and performance of a 30–40 GHz Josephson point contact mixer

The main goal in this study was to find the best mechanical structure of a point contact mixer for use on a radiotelescope. Besides good mechanical stability, a simultaneous low noise performance was desired.

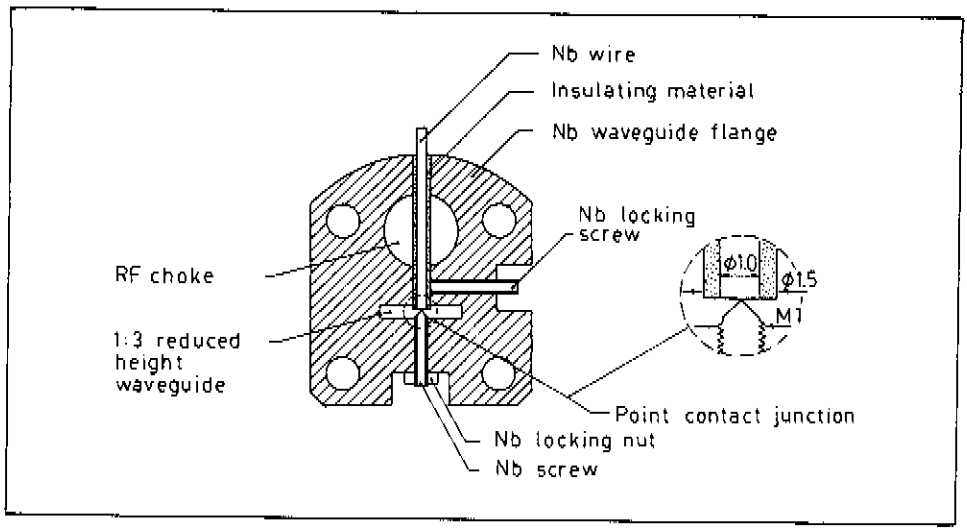

Figure 5. The waveguide flange construction used as a Josephson point contact mixer.

2.2.1. Junction preparation and mounting

The point contact was located in an 8 mm thick waveguide flange which is made of niobium (Figure 5). The construction was made as symmetrical as possible to prevent movement of the junction due to thermal contractions. In the flange there is a 1:3 reduced height waveguide where the point contact was formed. An insulated Nb wire was put into the waveguide from one side through a hole of 1.5 mm diameter and fixed stationary by a locking screw. Against the flat end of this anvil wire a sharply pointed screw was pressed from the other side to form the contact. Both the sharp point of the screw and the flat end of the anvil were prepared by grinding with fine emery paper. Normally no oxidization procedure was used but the surfaces could oxidize in air during the adjustment.

Much attention was paid to the insulating material of the anvil wire. It must have thermal expansion properties nearly the same as niobium, the linear expansion coefficient of which is 7×10^{-6}/°C at room temperature. Finally, for the insulating material a mixture of Araldite (30 %) and SiO_2 powder (70 %) was chosen [25]. The grain size of the SiO_2 powder used was <44 μm. The losses of the insulating material have not been solved, but the dielectric constant is evaluated to be $\epsilon_r \cong 3.5$ at 35 GHz. This insulating material was cast on Nb wire in a teflon mould of inner diameter 1.5 mm.

In the flange construction the insulated anvil wire acts as an IF port. To prevent the RF power coupling to the IF circuit this port was provided with a RF choke which consists of a three-sectional transmission line. The electrical lengths of the sections are $3\lambda/4$ at RF. The characteristic impedance of the low impedance sections is $Z_L \cong 15\ \Omega$ and that of the high impedance section $Z_H \cong 100\ \Omega$. Thus, the IF amplifier of 50 Ω input impedance is seen from the point contact as an impedance of only 0.1 Ω which can be omitted when examining the RF circuit. However, the losses of the insulating material have not been taken into consideration. At the low intermediate frequencies used this choke is of no consequence. A photograph of the mixer flange is shown in Figure 6.

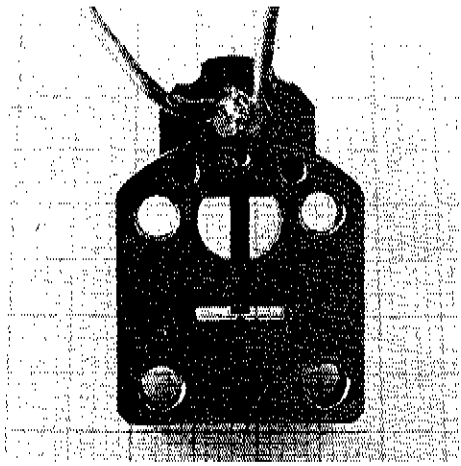

Figure 6. Photograph of a Josephson point contact junction in a waveguide flange.

The adjustment of the junction took place at room temperature without any fine-mechanical instruments. Experiments have shown that the adjustment of an unoxidized junction is noticeably more difficult than that of an oxidized one, and the adjustment to an arbitrary impedance does not easily succeed. It was attempted to adjust the impedance of the junction to values 0.5–5 Ω at room temperature. When cooling down this value may change a little. The junctions of higher impedance value were sensitive to shaking. Afterwards, when the junctions were opened, it was observed that the sharpened point was flattened. The diameter of the flattened area was 10–50 μm.

2.2.2. Microwave circuit

The RF impedance of the point contact is of the order of a few ohms, while the characteristic impedance of the WR-28 waveguide (26.5–40 GHz) is $Z_0 \cong 470\ \Omega$ at the »center» frequency 36 GHz. Thus, much attention must be paid to the impedance mathing. The first task was to reduce the heigh of the waveguide. This was done by a linear taper of length $2\lambda_g$, which reduces the height 1:3. At room temperature the following values were measured for this section at 36 GHz: attenuation = 0.5 dB, VSWR = 1.1.

When the point contact is located in the waveguide the parasitic series inductance must be taken into account in the equivalent circuit of the junction. Combining the inductance of a straight wire [21] and that of the point cone of the screw [45] the inductive series reactance is calculated to be $X_L \cong 40\ \Omega$ at the center frequency.

The RF power coupling to the junction was achieved by the resonator construction used by TAUR et al. [37]. That is, by using a capacitive tuning screw at the distance of $3\lambda_g/4$ ahead of the junction and a sliding short at the distance of $\lambda_g/4 - \lambda_g/2$ behind the junction. The tuning screw is a normal M1 brass screw, which is not adjustable in the cryostat. The optimum position of the tuning screw at room temperature could be found by observing the RF power coupling to a typical junction impedance, 3 Ω for example. A triple-screw tuner was also tried in order to broaden the bandwidth. This matching was, however, much more sensitive to cooling and was therefore given up. The short is a finger-shaped structure made of a 0.05 mm thick phosphor bronze sheet, in which the spring force presses the fingers against the broad walls of the waveguide. The short can be moved from outside the cryostat, when the mixer is cooled.

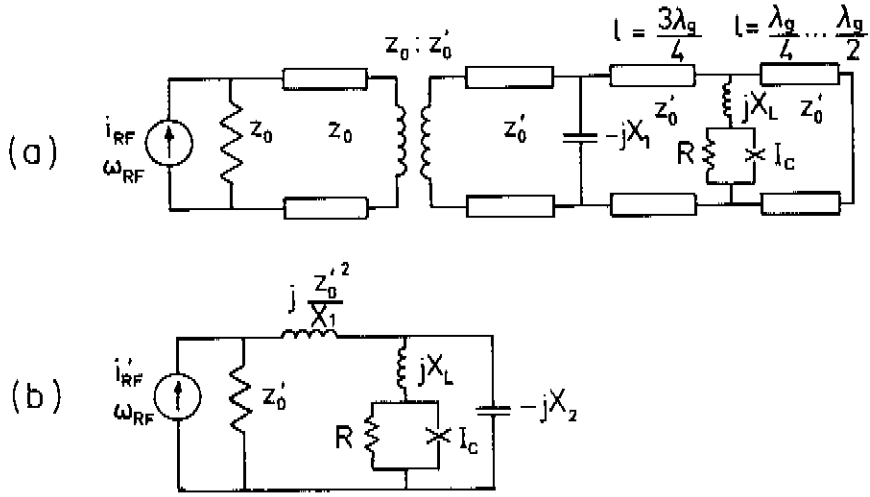

Figure 7. a) The equivalent RF circuit of the mixer, b) the same when reduced to the junction.

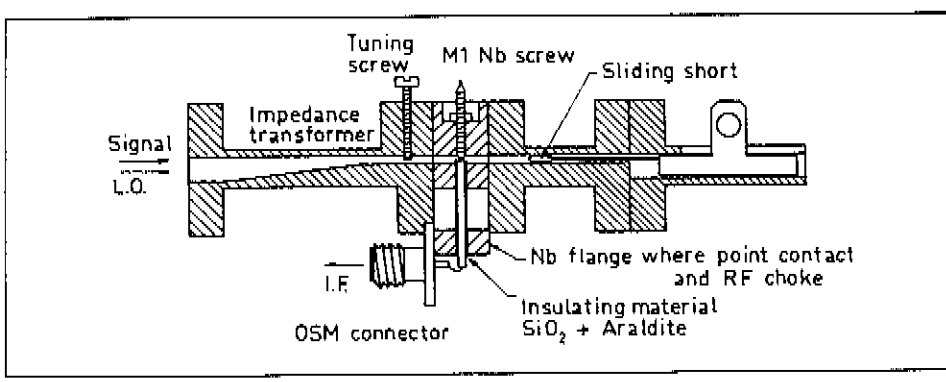

Figure 8. Cutaway view of the circuit realization.

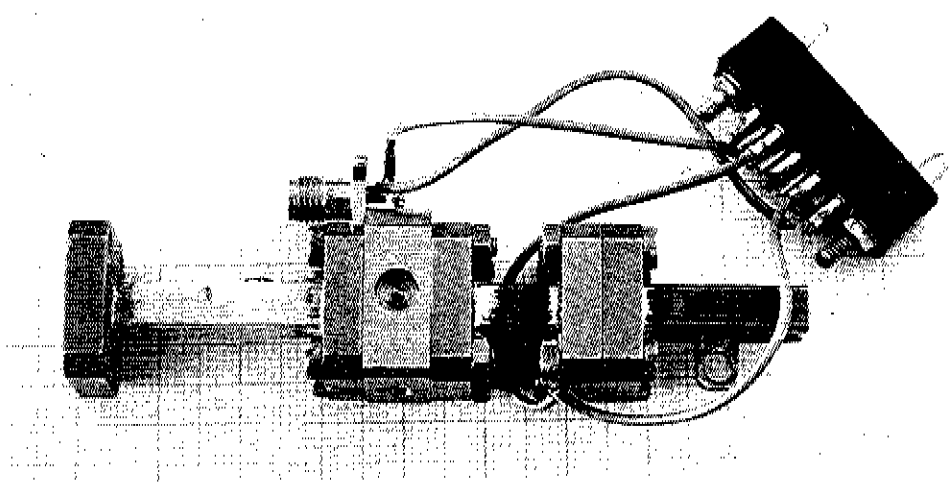

Figure 9. Photograph of the finished mixer.

An equivalent RF circuit for the resonator which was used in the design for calculating coupling and bandwidth is illustrated in Figure 7. In the equivalent circuit losses are not taken into consideration. Thus it gives too optimistic a picture about the power coupled to the junction and underestimates the bandwidth of coupling. Experiments have shown that the instantaneous bandwidth of the RF circuit described is 300–600 MHz depending on the impedance of the junction and the frequency. In Figure 8 the realization of the circuit is illustrated, and in Figure 9 a photograph of the finished mixer is presented.

2.2.3. Cryogenics

Two different cooling methods were used. In the beginning the mixer was cooled in a cryostat where the space between two vacuum shells was filled with liquid nitrogen and the inner space with liquid helium. The mixer was located in this inner space. The surface level of the liquid helium could be observed by means of a Nb wire resistance. To insure its survival the point contact was cooled slowly. First the junction was allowed to cool to the temperature of liquid N_2 (77 K) for 3–4 hours – the inner vacuum shell guarantees that the cool-down will occur slowly. Only after this time was He introduced to the cryostat. The helium is in direct contact with the mixer.

Later on, the mixer was cooled in a liquid He transportation dewar. The 5 cm neck of the dewar allows for direct immersion of the mixer from room temperature into liquid He or letting the mixer cool down first in the cold He gas above the liquid surface. In this way cool-down times from a few seconds to tens of minutes were possible.

2.2.4. Microwave sources and intermediate frequency system

The local oscillator power was supplied by a Gunn oscillator [24], which is mechanically tunable over the whole WR-28 waveguide band (26.5–40 GHz) and provides 100 mW of output power. In conversion loss measurements a second similar Gunn oscillator was used as a signal source and tuned for a frequency differing by the intermediate frequency from f_{LO}. The frequency difference was constant to better than 1 MHz/hour without any locking. The power from the Gunn oscillators was fed through attenuators and directional couplers into the cryostat. There was a copper-plated waveguide of german silver about 75 cm long ahead of the actual mixer. This waveguide caused an attenuation of about 0.5 dB to the signal.

The IF power was coupled from the mixer to the amplifier through a miniature coaxial cable with teflon dielectric. To improve the coupling, simple matching circuits were used in front of the amplifier outside the cryostat. At low IF's (e.g. 60 MHz) this matching circuit consisted of the transmission line mentioned above and a series inductance. This provided a perfect match over a few MHz bandwidth. At higher frequencies more complicated matching circuits were used, but because of the long cable before the circuit the matching normally was far from ideal. For IF amplification broad band bipolar transistor amplifiers were used. The highest f_{IF} used in the experiments was 2 GHz.

2.2.5. DC properties of the junctions

The *I-V*-characteristic was measured by normal four-lead technique (Figure 10). To prevent the coupling of the IF power to the DC circuit two 100 μH inductors were used, one in the current supply circuit, and the other in the voltage measurement circuit. At the same time these inductors prevent RF noise from getting to the junction from the

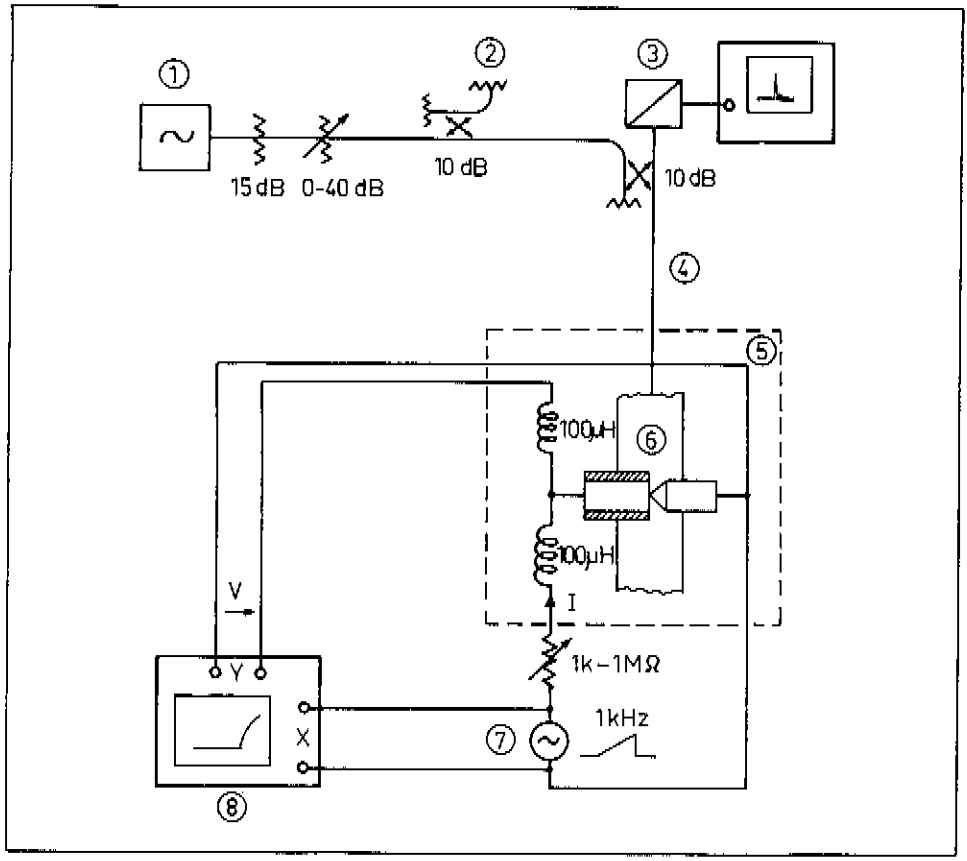

Figure 10. *I-V*-characteristic measurement set-up. 1) Gunn oscillator, 2) RF power and frequency measurement arm, 3) RF power coupling measurement arm, 4) waveguide, 5) liquid He vessel, 6) point contact in the reduced height waveguide, 7) current supply to the junction, 8) oscilloscope.

DC circuit. The DC current was supplied by a function generator through a variable high resistor. The voltage across the junction was measured with an oscilloscope. The overall measurement accuracy in *I-V*-characteristics was evaluated to be ±10 %.

Before measuring the step structure of the characteristic the power coupled to the junction was maximized by adjusting the sliding short and observing the reflected power with a spectrum analyzer. Optimum match always gave a return loss greater than 10 dB.

The *I-V*-characteristics of 28 junctions were experimentally measured. The critical current I_c and the resistance R (the inverse slope of the curve at high voltages) were measured without any RF power applied. From these quantities the »cut-off frequency» f_c of the junction can be calculated. When RF power was applied to the junction the power P_{LO} required to reduce the height of the zeroth voltage step to the value of $I_0 = I_c/2$ was measured. This value is the starting point when looking for the optimum value for mixing. Furthermore, the dynamic resistance R_{dyn} was measured from the *I-V*-characteristic.

The results of these DC measurements are given in Table 1. Special attention is drawn to the fact that f_c values of some junctions are above 1050 GHz, the theoretical value of Nb. Similar results are reported by ZIMMERMAN [45]. It is not easy to find an explanation for this phenomenon. On the other hand, some junctions had a very low f_c which

Table 1. Results of DC measurements.

Junction	$I_c/\mu A$	R/Ω	f_c/GHz	P_{LO}/dBm	R_{dyn}/Ω	Hysteresis
1	36	1.6	28	-40	1.6	
2	830	1.5	600	-35	1.5	
3	3200	0.30	460	-19	0.40	
4	70	6.7	230	-50	7.0	
5	36	2.8	49	-51	3.3	
6	900	2.1	910	-35		
7	3500	0.13	220	-24		
8	3050	0.73	1080			
9	1750	0.73	620	-28	0.75	
10	1600	0.74	570			x
11	3000	0.66	960			x
12	750	1.6	580	-29	2.0	x
13	8800	0.25	1060			
14	7400	0.26	930	-17		
15	7900	0.47	1800	-12	0.53	x
16	420	6.0	1220	-38		x
17	340	3.3	540	-38	4.0	x
18	300	4.0	580			
19	190	10	920	-25		
20	100	6.0	290			
21	420	3.2	650			x
22	280	7.2	970			
23	340	3.4	560			
24	5	40	96	-55		
25	2500	0.7	860	-20	1.0	
26	520	2.2	550			x
27	600	0.47	140	-32	1.8	x
28	9000	0.45	1960			

is due to the strong oxidation of these junctions. Furthermore, several junctions showed hysteresis. There is no apparent correlation between hysteresis and any characteristic value.

2.2.6. Conversion loss and noise temperature

The conversion loss of the mixer was measured with coherent signals using the set-up in Figure 11. The RF power was measured both with a spectrum analyzer and a thermistor power meter. The input flange of the cryostat was considered as the reference level of the input power to the mixer. The output power or IF power was measured with a spectrum analyzer and its reference level was the input of the IF amplifier. When defining the reference levels like this, the losses of the waveguide and IF cable are considered to be part of the conversion loss. The overall accuracy in conversion loss measurement was about ±1 dB.

The optimum operation point of conversion was found by changing the LO power and at the same time adjusting the bias current. Experiment showed that the optimum LO $P_{LO,opt}$ was within limits of ±3 dB the same as the power P_{LO} with which $I_0 = I_c/2$. The LO power required varied very strongly: −55...−10 dBm depending on the critical current of the junction. The LO power required by a good mixer was −40...−30 dBm.

By adjusting the bias current the conversion efficiency could be studied at different points of the *I-V*-characteristic. The maximum IF response for each step occurred half-

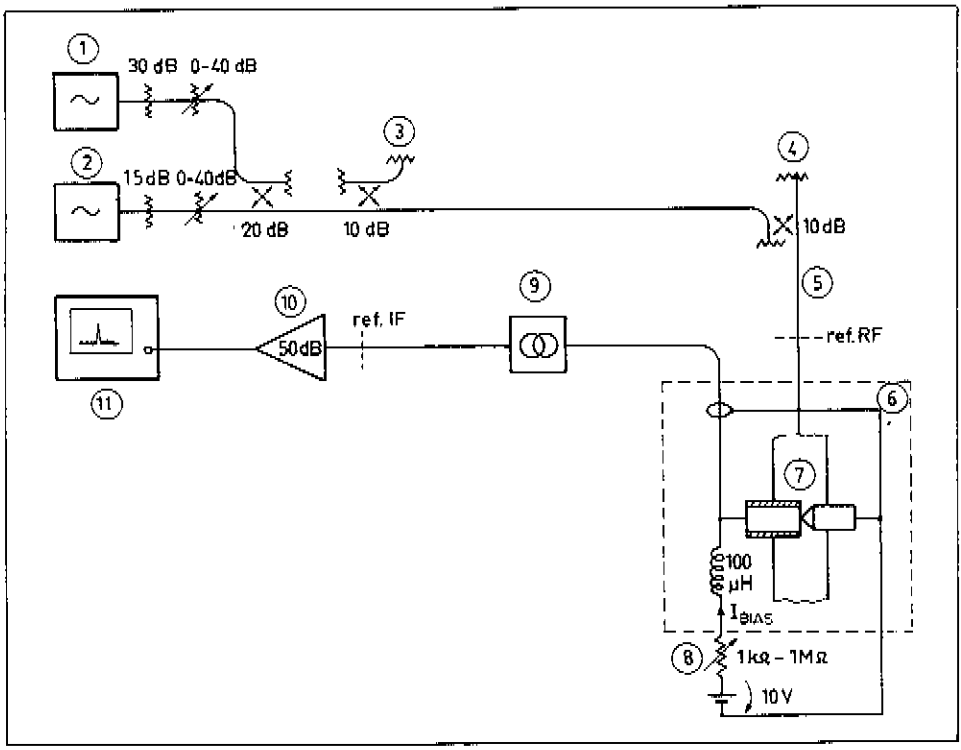

Figure 11. Conversion loss measurement set-up. 1) Signal source, 2) local oscillator, 3) RF power and frequency measurement arm, 4) power coupling measurement arm, 5) waveguide, 6) liquid He vessel, 7) point contact, 8) bias current supply, 9) IF matching circuit, 10) IF amplifier, 11) IF power measurement.

way between the steps. Generally the best conversion efficiency occurred between the zeroth and first step, but there were also exceptions: for some junctions the same maximum IF response occurred at four different steps. When mixing with hysteretic junctions the second or third step normally had to be used.

The dynamic range of the mixer was determined by finding the signal power at which the IF output deviated 3 dB from the linear response. The saturation level was normally 70... 50 dBm, about 20 dB below the LO power required, but great deviations also occurred.

The results of conversion loss measurements at $f_{IF} = 60$ MHz are given in Table 2 [31]. The best conversion loss values were 5 dB. An apparent correlation between high dynamic resistance and low loss can be seen. In addition, the best conversion loss values occur at normalized frequencies $\Omega = 0.04 - 0.16$ ($\Omega = f_s/f_c$) corresponding to the »cut-off frequencies» of 200 - 900 GHz. In conclusion, in order to achieve a good conversion result it is advantageous to adjust the junction to the highest possible impedance value within the limits caused by the stability requirement.

All results in Table 2 were measured at 36 - 37 GHz. However, similar results were obtained also at other frequencies between 30 and 40 GHz.

The junctions no. 1...17 were tested only with the 60 MHz IF system. Later junctions no. 18...28 were tested over a wider IF band. Depending on the junction, conversion losses of 15 - 25 dB were measured for several junctions up to $f_{IF} = 2$ GHz. However, at frequencies $f_{IF} < 200$ MHz there was too much disturbance as the screen room used

Table 2. Results of conversion loss measurements at f_{IF} = 60 MHz.

Junction	R_{dyn}/Ω	$P_{LO,opt}$/dBm	$I_{DC}/\mu A$	Ω	L_C/dB	Hysteresis
2	1.5	-35	470	0.060	15	
4	7.0	-55	46	0.156	7	
6		-35		0.040	5	
8			1750	0.033	11	
9	0.75	-28	1100	0.058	14	
12	2.0	-29	540	0.062	7	x
14		-17	3900	0.039	10	
16		-38	220	0.030	15	x
17	4.0	-38	190	0.067	5	x

earlier was no longer available. The response for any junction was quite flat (±1 dB) over the whole IF band 200–2000 MHz. Several dB's of the high conversion loss in these experiments can be explained by considerable IF cable loss and poor matching (see section 2.2.4.).

Only a few measurements of the noise temperature were performed (all at f_{IF} = 60 MHz) because of the lack of suitable equipment. These few measurements were made by normal *Y*-factor technique using a neon discharge tube as a noise source. The noise power in the IF amplifier output was measured by a tunable field strength meter with input bandwidth of about 700 kHz. The best result was achieved with a hysteretic junction (no. 17) when biased to the third step. The receiver noise temperature was measured to be 1000 K in double sideband operation including the noise of the IF amplifier (T_{IF} = 130 K).

2.2.7. Mechanical stability of the mixer

The mechanical stability of the mixer was studied during the DC measurements. The junctions were tested against continuous vibration and shock. The junctions were observed to be very stable when the contact resistance was $R \leqslant 5\ \Omega$. With higher resistance values some changes in the critical current and in the slope of *I-V*-curve occurred.

In addition, the stability of junctions against temperature cycling between 4.2 K and 295 K was studied. Most junctions kept their Josephson behaviour in spite of several coolings, but some changes in the *I-V*-characteristics occurred. Some junctions opened when the temperature rose from 4.2 K to 295 K. The junctions generally withstood quick cooling very well. The shortest cool-down times were of the order of one minute.

3. SCHOTTKY DIODE MIXER

3.1. Schottky diodes for millimeter waves

The Schottky diodes for millimeter wave mixing are nowadays mostly fabricated on n-type epitaxial GaAs [35], [43], [44]. Classical silicon has too low an electron mobility, while the epitaxial technologies for high mobility semiconductors such as InAs and InSb are not yet developed enough. The metal contact is usually a thin platinum layer followed by gold. The impurity may be for example Te, Ge or Sn; and the concentrations in the epilayer are normally $2 \times 10^{16} - 5 \times 10^{17}$ cm^{-3}. Figure 12 shows a typical millimeter wave diode chip structure.

The principal factors limiting the performance of Schottky-barrier diodes are the barrier capacitance C_j shunting the nonlinear barrier resistance R_j, and the spreading (series) resistance R_s which is in series with the barrier (Figure 13). The parasitics R_s and C_{j0} (C_j at zero bias voltage) define the cut-off frequency f_c which is one of the most important figures of merit in describing the high frequency quality of a mixer diode:

$$f_c = \frac{1}{2\pi R_s C_{j0}} . \tag{8}$$

Typical values of the parasitics and the cut-off frequency for the best millimeter wave Schottky diodes are: $R_s = 4 - 10\ \Omega$, $C_{j0} = 5 - 15$ fF and $f_c = 2.5 - 5.0$ THz at room temperature.

Conduction in Schottky-barrier diodes is due to a combination of two different electronic processes, thermionic emission and field emission [26]. Thermionic emission con-

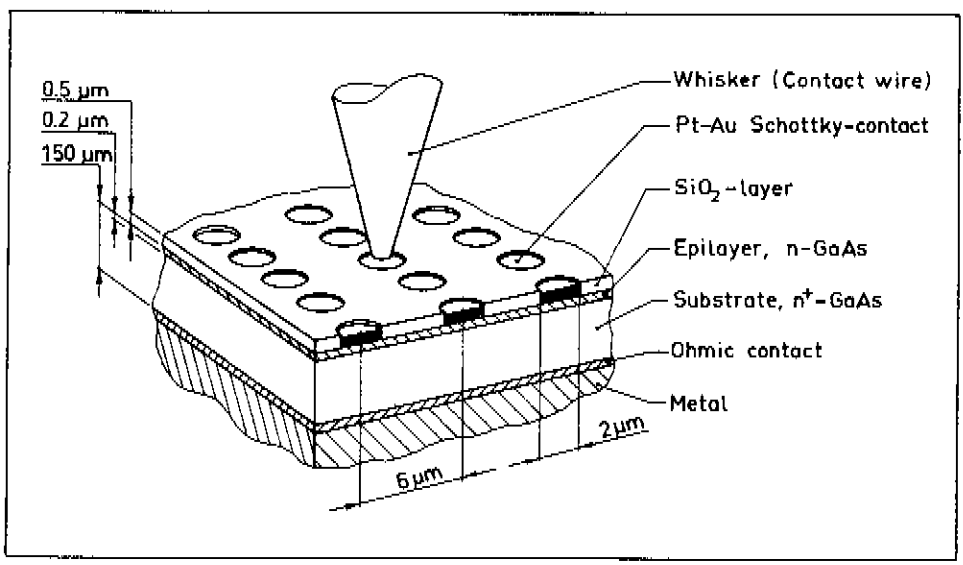

Figure 12. A typical Schottky diode chip.

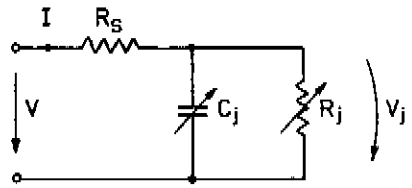

Figure 13. Equivalent circuit for a Schottky diode.

sists of electrons with sufficient thermal energy to cross the barrier, while field emission consists of electrons which tunnel through the barrier. The relative proportion of current transport due to these two processes depends on the physical temperature of the diode T, the doping density N_D and the effective mass of the electrons m^*. In general, the I-V-characteristic of a Schottky diode may be written (assuming negligible R_s)

$$I = I_{00} \exp(V/V_0) \tag{9}$$

for $I \gg I_{00}$, where I_{00} is the saturation current. It has been shown that for thermionic-field emission [26]

$$V_0 = \frac{E_0}{e} \coth\left(\frac{E_0}{kT}\right) , \tag{10}$$

where

$$E_0 = \frac{eh}{4\pi}\left(\frac{N_D}{\epsilon_0 \epsilon_r m^*}\right)^{1/2} , \tag{11}$$

and k is Boltzmann's constant, ϵ_0 is the dielectric constant of vacuum and ϵ_r is the relative dielectric constant of the semiconductor. For the field emission case (high doping and/or low temperature)

$$V_0 = \frac{E_0}{e} \tag{12}$$

and for the thermionic emission case (high temperature and/or low doping)

$$V_0 = \frac{kT}{e} . \tag{13}$$

Besides the general equation (9) the I-V-characteristic often is written ($I \gg I_{00}$)

$$I = I_{00} \exp\left(\frac{eV}{\eta kT}\right) , \tag{14}$$

where η is the ideality factor having values from 1 to 10 depending on temperature and doping. Figure 21 shows I-V-curves of diodes used in this work at three different temperatures.

Using Equations (9) and (14), the barrier resistance is calculated to be

$$R_j = \left(\frac{dI}{dV}\right)^{-1} = \frac{V_0}{I} = \frac{\eta kT}{eI} , \tag{15}$$

because $\partial I_{00}/\partial V \ll I_{00}/V_0$ for Schottky diodes. The reciprocal of R_j is the barrier conductance $G_j = 1/R_j$. The application of a voltage $V = V_{DC} + V_{LO}\cos\omega_{LO}t$ gives rise to a time dependent conductance given by

$$g(t) = \frac{I_{00}}{V_0}\exp\left(\frac{V_{DC}}{V_0}\right)\exp\left(\frac{V_{LO}}{V_0}\cos\omega_{LO}t\right)$$

$$= \frac{I_{00}}{V_0}\exp\left(\frac{V_{DC}}{V_0}\right)\left[I_0\left(\frac{V_{LO}}{V_0}\right) + \sum_{n=1}^{\infty} 2I_n\left(\frac{V_{LO}}{V_0}\right)\cos n\omega_{LO}t\right]$$

$$= g_0 + 2g_1\cos\omega_{LO}t + 2g_2\cos 2\omega_{LO}t + \cdots , \tag{16}$$

where the $I_n(x)$ terms are modified Bessel functions.

The frequency conversion in a mixer diode is due to the nonlinear conductance and, thus, the conversion loss can be calculated by using conductances g_n [39]. When the series resistance is also taken into account an extra factor for the conversion loss is gotten. This minimum loss can be expressed in terms of the cut-off frequency by:

$$L_p = 1 + 2\frac{f}{f_c} . \tag{17}$$

A strict theory for the conversion loss and noise temperature of the Schottky diode mixer is presented for example in Reference [10].

3.2. Design of a cooled 75–120 GHz Schottky diode mixer

This mixer was designed for a receiver to be used for radioastronomical observations on a 13.7 m radiotelescope. To satisfy as many radioastronomers as possible one mixer should cover the whole WR-10 waveguide band (75–115 GHz) thus eliminating time consuming mixer and/or receiver changes. Other goals were a state-of-the-art noise performance and a high reliability.

3.2.1. Waveguide mount

In order to find the best material for the waveguide mount a series of experiments were carried out in which the conductivity of several metals was measured at different temperatures (Table 3). These measurements were made using the four-lead technique. OFHC copper was chosen because of its superior DC conductivity at low temperatures.

Table 3. Measured DC resistivities of some metals.

Metal	ρ(295 K)/$\mu\Omega$ cm		$\frac{\rho\,(295\text{ K})}{\rho\,(77\text{ K})}$	$\frac{\rho\,(295\text{ K})}{\rho\,(4.2\text{ K})}$
	measured	theor. for pure metals		
OFHC-Cu	1.9	1.72	8.3	200
OFHC-Cu (annealed)	1.9	1.72	8.3	260
Te-Cu	2.1	1.85–1.90	5.2	14
Te-Cu (annealed)	2.1	1.85–1.90	5.3	16
Au	2.6	2.20	4.4	34
Brass	7.4	~7	1.7	2.2

Annealing increases the low temperature conduction slightly more. Furthermore, it is known [1] that through annealing the high frequency losses at room temperature can be reduced because the rough surface layer is modified. However, the final waveguide mounts were not annealed because the resulting detrimental tarnish films need to be removed by etching, and after all this the final surface conductivity might not be better than the original.

In the above discussion the anomalous skin effect [28] appearing at low temperatures and high frequencies has not been taken into account. In a normal case the conductivity depends on the mean free path of the electrons. For high conductivity metals such as Cu, the mean free path increases very rapidly when the temperature decreases [16] and can exceed the classical skin depth at very low temperatures and high frequencies. In this case the surface resistance no longer depends on the DC conductivity but depends on other material parameters and frequency [28]. Therefore, it might be possible to find better metals than Cu for construction material of a cryogenic waveguide.

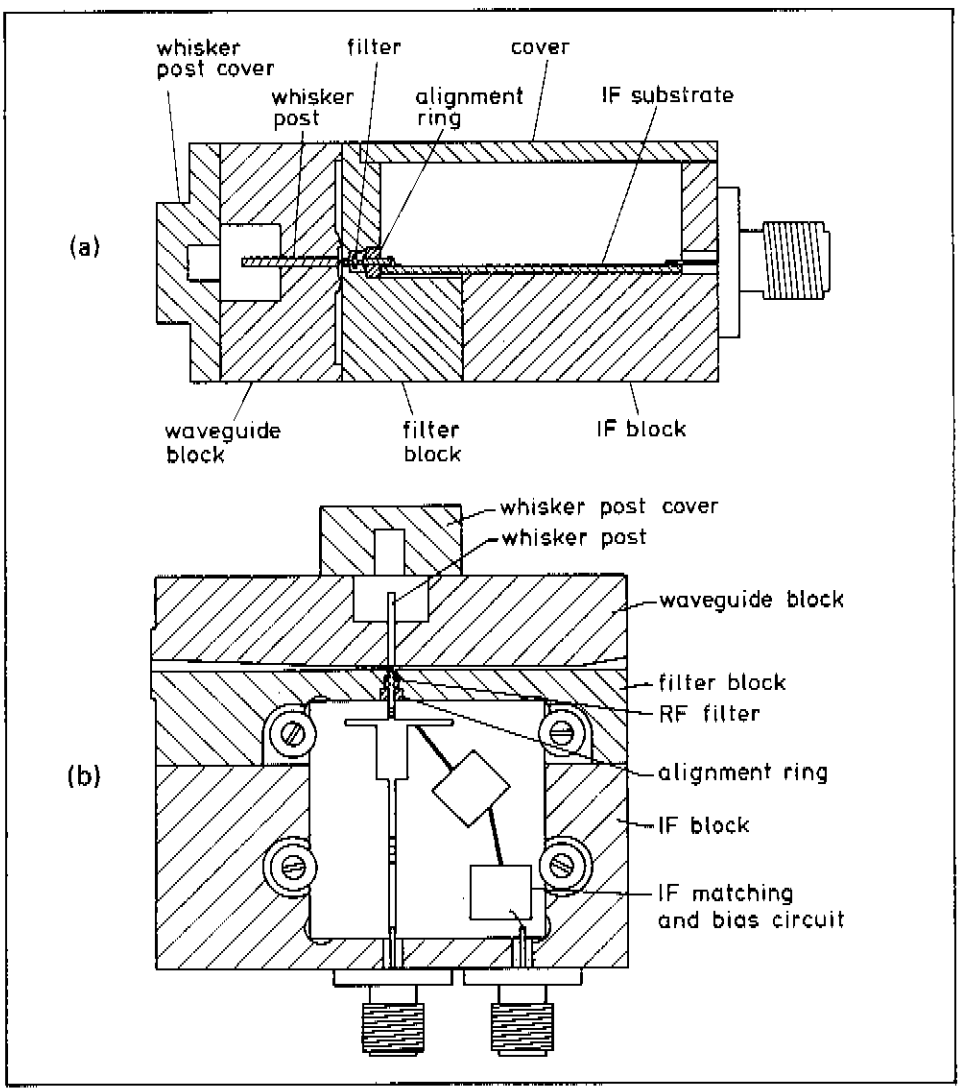

Figure 14. Mixer block, a) side view, b) upper view.

The mixer block (Figure 14) consists of three separate pieces to provide easy access to any point of the mixer. The waveguide section consists of two blocks, one having a flat surface and the other the waveguide channel. In order to have good electrical contact between the two blocks the contact edges make an acute angle as shown in Figure 14a.

The transition from full height WR-10 waveguide to one-quarter height waveguide (2.54 mm x 0.30 mm) is made by a linear taper of 23 mm length. This length is 3.5–8.0 λ_g at frequencies 75–120 GHz respectively. An insertion loss of 0.2–0.3 dB was measured for this taper.

3.3.2. Backshorts

The most commonly used sliding backshort type in mm-wave mixers is a contacting short [6], [14], [18]. That type of a short was also used in the Josephson point contact mixer described earlier.

However, to avoid the wear characteristic of contacting backshorts, a non-contacting short is necessary in a wide band mixer where the operation frequency has to be changed frequently. Furthermore, to eliminate the pass-band at 2nd harmonic frequencies inherent in conventional $\lambda/4$ designs, new empirically and theoretically designed shorts were built [32].

To fit into a reduced height waveguide the backshorts were made of 0.25 mm thick copper-plated brass and insulated from the waveguide by a 19 μm thick mylar tape. Figure 15a shows the structure of the shorts consisting of five alternating low and high impedance sections. The empirical design was approached by using the experience concerning backshorts and RF chokes gained in earlier millimeter wave mixer work. Also, a computer program was developed to design backshorts [2]. In the program the backshort is modeled as a series of alternating »pi» and »tee» sections with fringing capacitances in each junction (Figure 15b). These reactances are further lumped to give the final LC filter (Figure 15c). This filter is then treated using standard Chebyshev techniques [22] to produce the desired response. The dimensions of these designs as well those of the $\lambda/4$ design are shown in Table 4.

Table 4. Dimensions 4–1 of the backshorts (in mm).

Design	Section			
	4	3	2	1
$\lambda/4$	0.51	0.84	0.56	0.91
Empirical	0.65	0.51	0.44	0.86
Chebyshev	0.24	1.12	0.24	0.46

New designs were tested before construction using a second program which plots theoretical VSWR vs. frequency. Both programs adjust for the guide being partially filled with dielectric material. Figure 16 shows the theoretical VSWR for different designs at frequencies 70–260 GHz.

The backshorts were tested at frequencies 75–116 GHz and 204–232 GHz in a test waveguide similar to the waveguide channel in the cooled mixer. A thin sheet of copper pressed between two waveguide flanges was used as a reference short. The measurement set-up at the 2nd harmonic band is shown in Figure 17. The output of the BWO sweeper was doubled using a Schottky diode frequency multiplier [7] providing output power

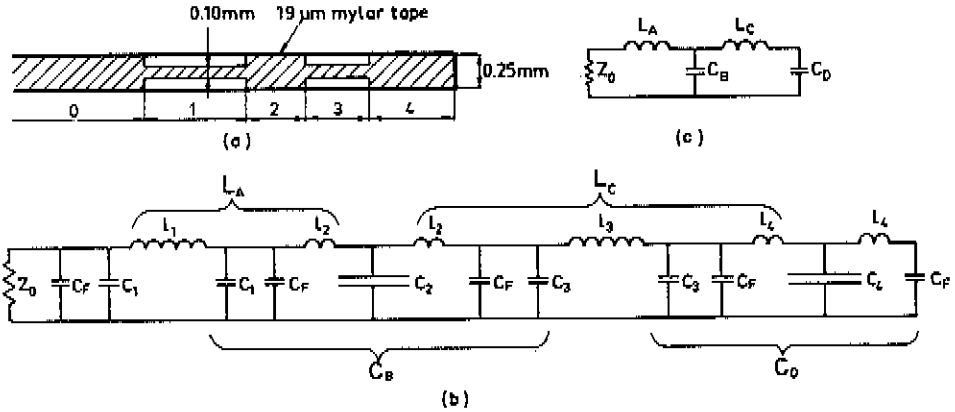

Figure 15. a) Non-contacting backshort for reduced height WR-10 waveguide, b) quasi-lumped circuit, c) lumped circuit.

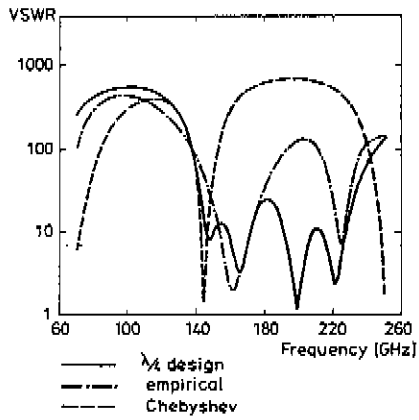

Figure 16. Theoretical VSWR curves.

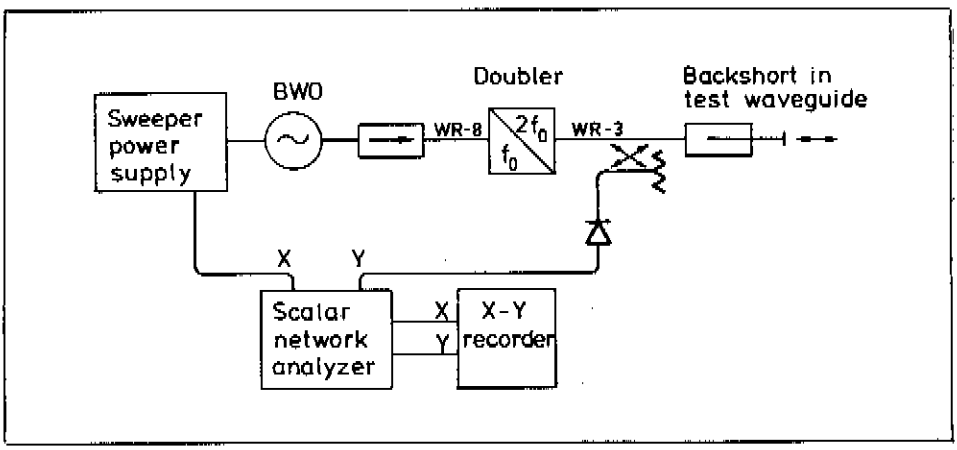

Figure 17. Measurement set-up for frequencies over 200 GHz.

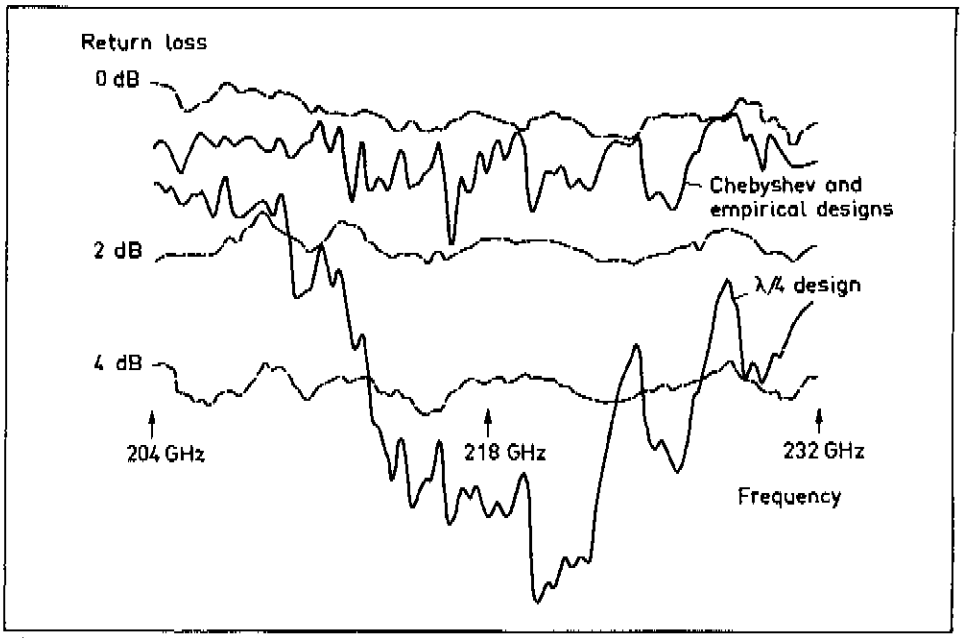

Figure 18. Measurement results at 2nd harmonic frequencies.

1–5 mW over the swept frequency band of 204–232 GHz. Directional couplers of 20 dB coupling and 40 dB directivity were used to measure the reflected wave. The detected signals were analyzed by a scalar network analyzer.

At frequencies 75–116 GHz return losses of 1.0 to 0.8 dB (including twice the loss of the test guide) were measured, respectively, for the empirical and Chebyshev designs. The results reveal that the VSWR is between 60 and 90 (+100 %, −10 %) for the empirical and Chebyshev designs and 30 to 90 for λ/4 design. At the 2nd harmonic frequencies the VSWR for the empirical and Chebyshev designs is approximately the same as at the fundamental frequency but the λ/4 short now has a VSWR only of 4–20 (Figure 18). Before copper-plating the same shorts yielded on average 0.2 dB higher return loss.

3.2.3. RF filter

Both suspended microstrip ([14], [18], [43]) and coaxial ([20], [40]) RF filters are used in mm-wave Schottky mixers. Both types are suitable for cooling [14], [20].

The reason to design a new RF filter was to improve the frequency response. The RF filter, shown in Figure 19, is a coaxial structure consisting of alternating low and high impedance sections. It is a low-pass filter which confines the fundamental and second harmonic frequencies to the mixer waveguide. It has been analyzed with a computer program to present a short near 120 GHz and be reactive from 75 to 225 GHz [29]. The frequency response was checked with a 10:1 scale model (Figure 20). The inferred insertion loss is greater than 15 dB above 80 GHz and 20 to 40 dB from 88 to 120 GHz scaled frequency. The impedance versus frequency of the scaled model agrees excellently with the computer results at scaled frequencies 80–120 GHz.

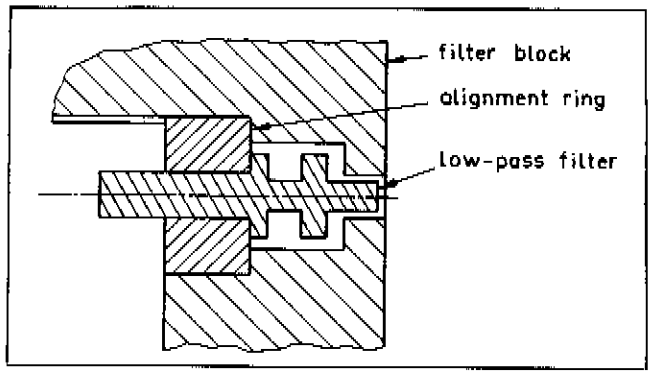

Figure 19. RF filter.

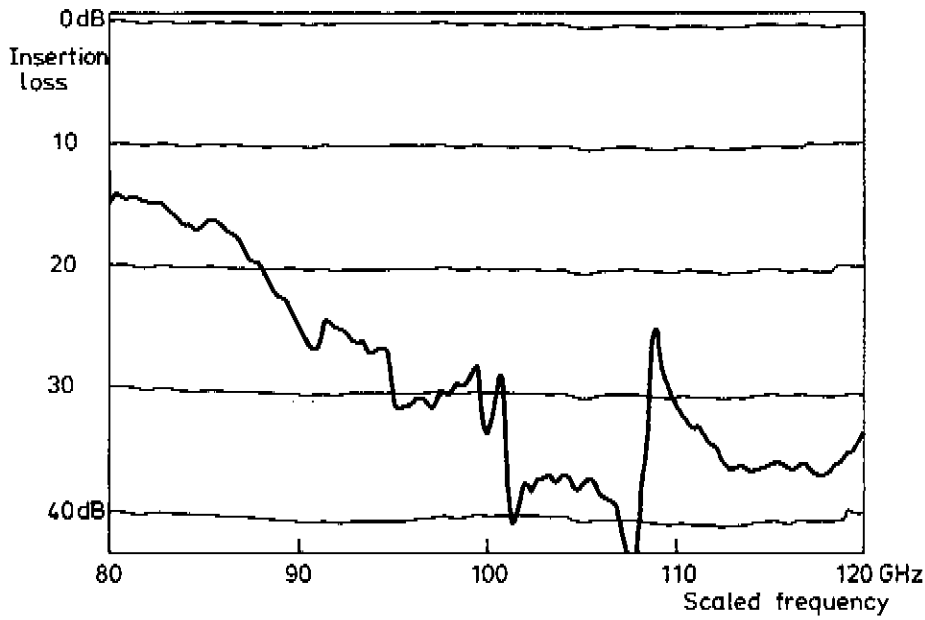

Figure 20. Insertion loss of the 10:1 scaled model filter.

The inner conductor of the filter was machined from OFHC copper and is insulated by a machineable ceramic (macor) ring. The ring, with $\epsilon_r = 5.7$ and low-loss tangent (.007 at 8.6 GHz), was machined to 5 micron tolerances with no need for postmachining firing.

3.2.4. Diodes

As a mixing element two kinds of Schottky diodes have been used. The diodes were fabricated on n-type epitaxial GaAs by M. SCHNEIDER at Bell Laboratories. The first type of diode is designed for room temperature use. The doping is relatively high (2×10^{17} cm^{-3}) in the epilayer. The junctions are circular Ø4.3 μm. At 295 K the DC series resistance and ideality factor are 6–9 Ω and 1.17–1.20, respectively. A typical set of *I-V*-characteristics of this type of diode at different temperatures is shown in Figure 21a. The second type is especially designed for cryogenic operation. The epilayer doping density is only 5×10^{16} cm^{-3} within the first 1000 Å. The junctions have 'bathtub' form: 2.5 μm x

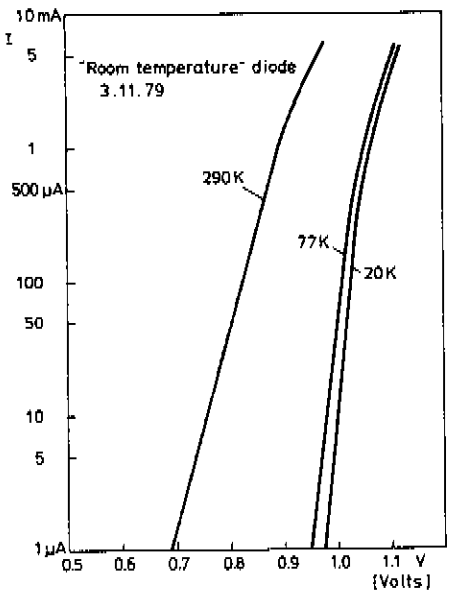

Figure 21a. *I-V*-characteristic of the »room temperature» diode.

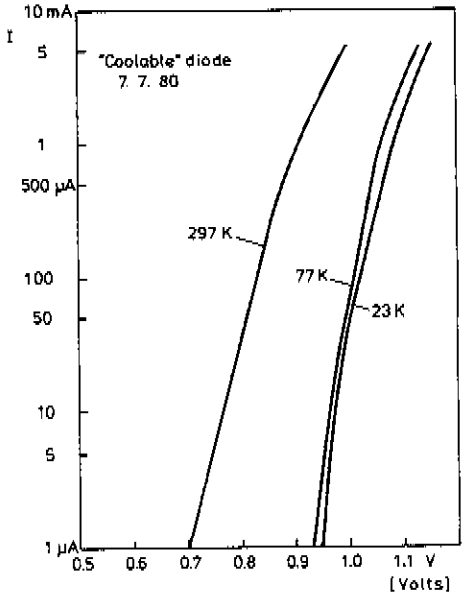

Figure 21b. *I-V*-characteristic of the »coolable» diode.

4.4 µm. At 295 K typical DC series resistance values and ideality factors are 5–6 Ω and 1.11–1.15, respectively. The *I-V*-characteristic (Figure 21b) at low temperatures is not a simple exponential but a combination of several exponential functions. Therefore, the conduction in this diode can not be explained using the thermionic-field emission theory alone. The reason for this discrepancy is not known at present [34].

The diode chip, 0.28 mm x 0.28 mm x 0.13 mm, is soldered to the end of the RF filter. The upper surface of the diode array is flush with the waveguide wall. One of the diodes is contacted using a short gold-plated Ø 12 µm phosphor bronze whisker. The whisker wire is soldered to a brass post which is pressed into the opposite waveguide block.

3.2.5. IF matching and bias circuits

The other end of the RF filter is connected to the microstrip matching and bias network with a 6 µm gold ribbon. The ribbon allows small displacements due to differential thermal contraction upon cooling.

In some mm-wave Schottky mixers the IF matching is omitted [20] without any great harm, because cooled system IF reflection losses even of a few dB's do not contribute significantly to the receiver noise temperature. At room temperature the matching is more important and usually a simple λ/4 transformer is used [40]. The DC bias to the diode is usually fed through a bias-T. To optimize the total receiver performance new circuits were designed for this cooled mixer to match the IF port and to avoid the use of a bias-T.

In order to design a matching circuit one first has to carry out the difficult task of evaluating the IF impedance of the mixer. The IF impedance is a combination of a LO and DC biased diode impedance plus the RF filter impedance. The measurements have shown that the IF impedance depends on the LO power, DC bias, frequency and backshort position (in other words: on the RF impedance) in a given mixer mount.

Without any matching the VSWR in this mixer using a »coolable» diode is between 5 and 12 at f_{IF} of 4.5–5.0 GHz when the mixer is tuned for the best double sideband (DSB) receiver noise temperature at frequencies 75–120 GHz. However, because of the high VSWR, it is unclear whether the LO power and DC bias in the above experiment have been adjusted to the optimum values for the diode noise performance, or just those values which best compensate matching defects.

Anyway, in the lack of any better approach, the IF impedance was evaluated as follows. At the operation points mentioned above the *I-V*-curve of the pumped diode was measured and found to have in most cases a slope of between 150 Ω and 300 Ω; on average 200 Ω. The resistance R_d was then assumed to represent the total diode IF impedance. Next the mixer was taken from the dewar to a network analyzer set-up and the IF impedance seen at the far end of the RF filter was measured when the diode was only DC biased to represent a 200 Ω resistor, see Equation (15). From the resulting IF impedance the filter impedance can be solved. The equivalent circuit in Figure 24a simulates reasonably well the measured impedance which for its part agrees well with the computed results. The component values in the model of Figure 22a are C_{ch} = 1 pF and L_{ch} = 0.35 nH.

The IF impedance, Z_{in} = (5.7 – j23.3)Ω at 4.75 GHz, is matched to 50 Ω (Figure 22b) by a microstrip matching circuit. Many different types of circuits were designed and tested. The best results were obtained with networks consisting of a transmission line making the impedance real at the center frequency 4.75 GHz, followed by a parallel resonator and one- or two-section quarter-wave-transformer. Figure 23 illustrates the equivalent circuit of the latter design.

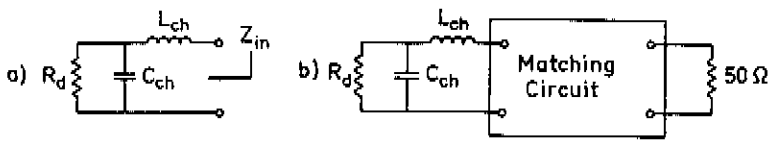

Figure 22. a) Equivalent circuit of the IF impedance and b) its matching.

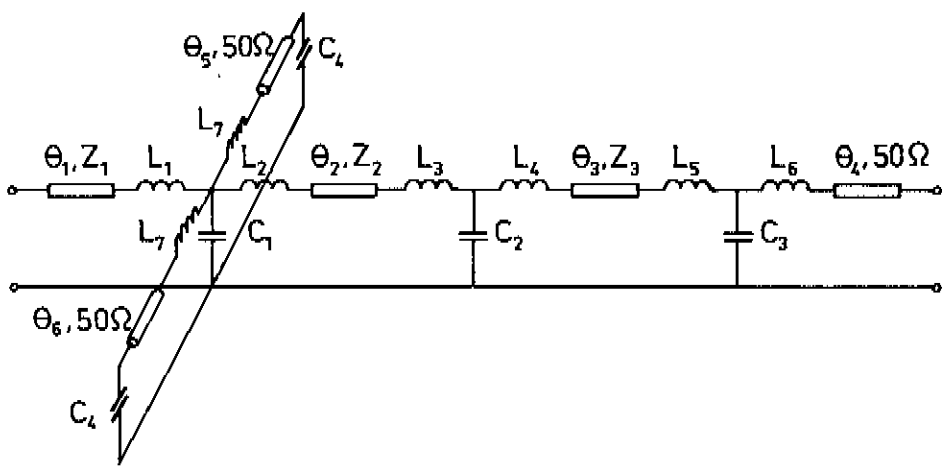

Figure 23. Equivalent circuit of the matching network (inductances and capacitances are due to discontinuities in the microstrip).

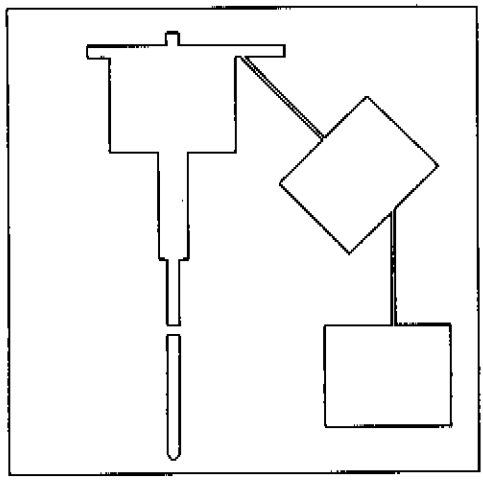

Figure 24. IF matching and bias circuit.

Receiver tests have shown that the mixer noise performance is far better with a matching circuit described above than without it. However, so far, the matching achieved does not fulfil the requirement of a 500 MHz instantaneous IF bandwidth. The reason is, firstly, that R_d values from 150 Ω to 700 Ω have now been measured at the optimum operation points and, secondly, that the diode IF impedance seems not to be purely resistive. This reveals parametric effects to be present in the frequency conversion. Nevertheless, the resulting bandwidth of 250 MHz or more (VSWR $\leqslant$ 2) at most operation points makes this mixer very usable in radioastronomical observations.

The matching circuit is fabricated by chemical etching on an alumina substrate and integrated with a low-pass filter for DC biasing (Figure 24). Alumina material was chosen because its high dielectric constant leads to a compact circuit. The conductor and ground plane are either Cu or Au.

3.2.6. Room temperature results

Photographs of the finished mixer are shown in Figure 25. Altogether 5 similar units have been fabricated so far, but only a few series of room temperature tests have been carried out. Preliminary results are shown in Table 5 [33]. The measurements at 1.4 GHz

Table 5. Room temperature results.

f_{LO}/GHz	Room temp. diode Mixer no. 2/1.40 GHz		Room temp. diode Mixer no. 3/4.75 GHz		Coolable diode Mixer no. 2/4.75 GHz	
	T_{MDSB}/K	L_C/dB	T_{MDSB}/K	L_C/dB	T_{MDSB}/K	L_C/dB
75	385	5.9	440	6.3	360	6.4
80	315	5.4	430	6.0	520	6.9
85	370	5.8	500	6.5	510	6.9
90	310	5.1	–	–	–	—
95	490	5.8	475	6.0	440	6.9
100	455	5.9	–	–	505	7.1
105	–	–	–	–	–	—
110	410	6.4	545	7.2	530	7.1
115	355	6.1	595	7.4	590	7.0
120	395	5.7	–	–	–	—

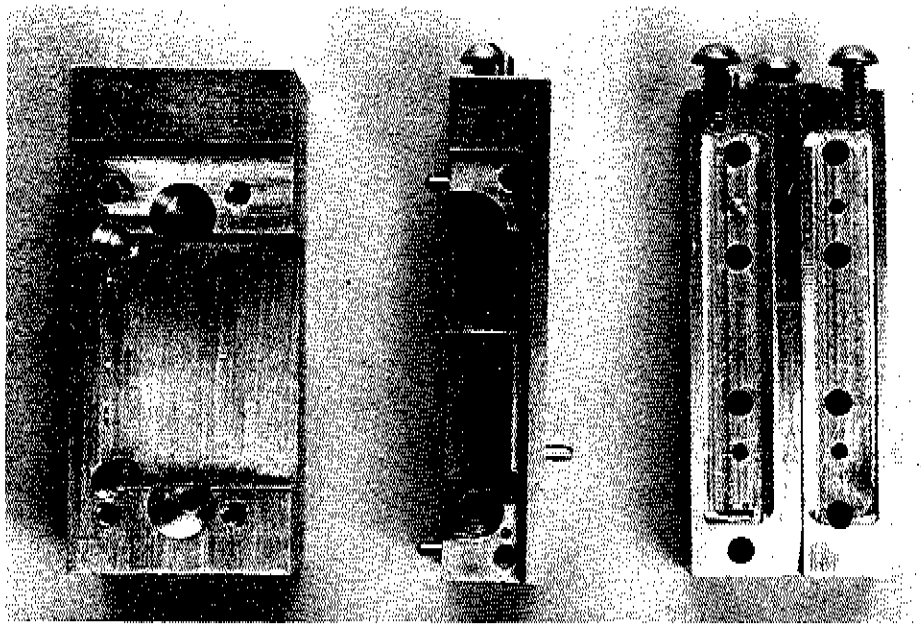

Figure 25a. The three pieces of the mixer block.

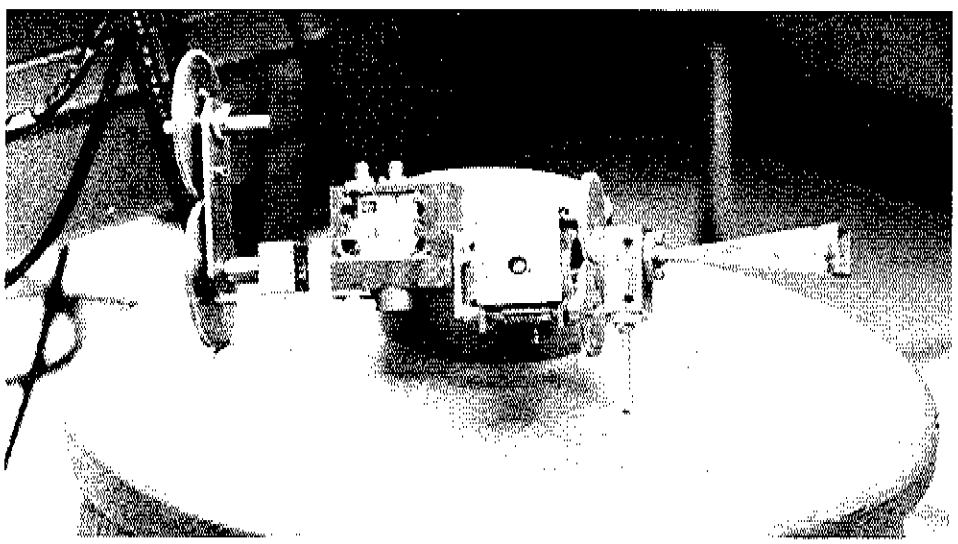

Figure 25b. A finished mixer assembled together with a feed horn, ring-filter and backshort moving mechanism.

IF were made with mixer no. 2 with a suitable matching circuit. At 4.75 GHz IF the measurements were carried out with mixer no. 3 having a room temperature diode and with mixer no. 2 having a coolable diode. In all these measurements a ring-filter was used to inject the local oscillator power. The performance of the ring-filter is as follows: 5–7 dB and 0.4–0.6 dB insertion loss for the LO and signal, respectively. Typical LO power into the mixer was 1–5 mW.

All measurements were double sideband measurements employing the Y-factor method using 295 K and 77 K loads in front of the feed horn (see Appendix A). The IF noise temperature was measured using the same technique at the input of the IF system. The measurement results are as follows:

$$T_{\mathrm{RDSB}} = (L_{\mathrm{F}} - 1)T_{\mathrm{room}} + L_{\mathrm{F}}T_{\mathrm{MDSB}} + L_{\mathrm{F}}L_{\mathrm{DSB}}T_{\mathrm{IF}} \tag{18}$$

and

$$L_{\mathrm{DSB}} = \frac{L_{\mathrm{s}}L_{\mathrm{i}}}{L_{\mathrm{s}} + L_{\mathrm{i}}}\,, \tag{19}$$

where L_{F} = 0.5...0.7 dB (including the ring-filter and feed horn), T_{room} = 295 K, and L_{s} and L_{i} are signal and image conversion losses. Further it is assumed that (the »worst case» assumption)

$$L_{\mathrm{C}} = L_{\mathrm{s}} = L_{\mathrm{i}} = 2L_{\mathrm{DSB}}\,. \tag{20}$$

During the room temperature tests no single sideband (SSB) filter was available, and therefore the mixer was always tuned for best DSB noise temperature using a signal-to-noise meter. Thus, only DSB noise temperatures are quoted, because the SSB noise temperature depends on the image load temperature and thus the exact system configuration (Appendix A). Additionally, this mixer has roughly equal conversion losses in the two sidebands when the system is tuned up for best DSB noise temperature.

3.3. Spectral line receiver for 75–120 GHz

The mixer described above is currently used in a cooled spectral line receiver on the FCRAO 13.7 m radiotelescope. Thus far, with this receiver, mapping of interstellar clouds has been carried out using spectral lines ^{12}CO (J = 1–0) at 115.27 GHz, ^{13}CO (J = 1–0) at 110.20 GHz and SiO (J = 2–1, v = 1) at 86.24 GHz. Also some extragalactic work has been done. The receiver is also suitable for continuum observations.

The total receiver front end is briefly described, because the evaluation of the cooled mixer performance is impossible without knowing the system configuration.

3.3.1. Quasi-optical feed system

The signal coming from the sky via the Cassegrain antenna is fed to the feed horn through a quasi-optical system [9], [29] (Figure 26a). This system allows the following operations: switching the beam between main and reference positions; calibration of the receiver with hot and cold loads; optimization of the receiver noise temperature through the use of the calibration chopper along with a signal-to-noise meter; and selection of the operation mode between either SSB or DSB.

The secondary focus of the telescope is near the beam switching chopper. An ellipsoidal mirror collimates the beam from the secondary focus, or from the hot (295 K) or cold (77 K) loads for the Michelson type interferometer filter (Figure 26b). This filter utilizes two thin (0.4 mm) quartz beamsplitters and an adjustable corner reflector to filter out the image sideband and terminate it at 77 K thus minimizing the receiver noise temperature in the SSB mode. The image rejection is 19 dB when the filter is tuned for ^{12}CO at 115.27 GHz in the upper sideband (USB).

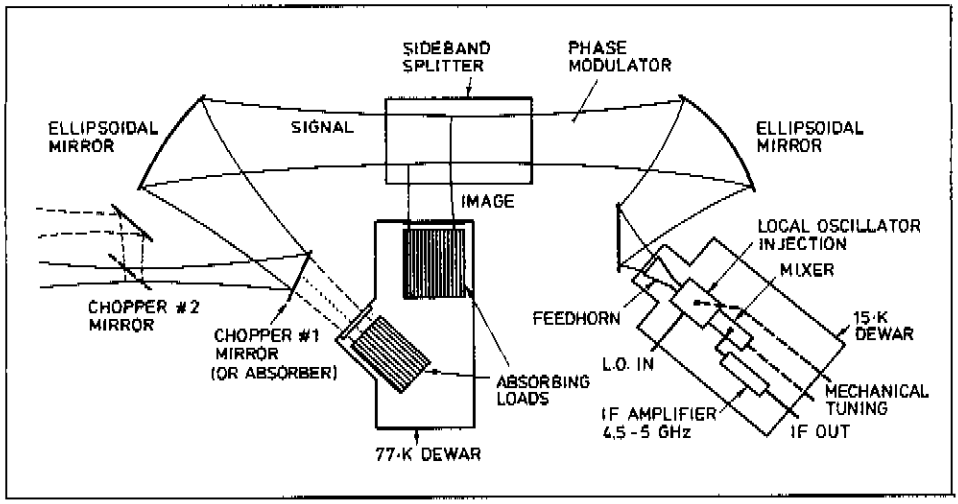

Figure 26a. Quasi-optical feed system.

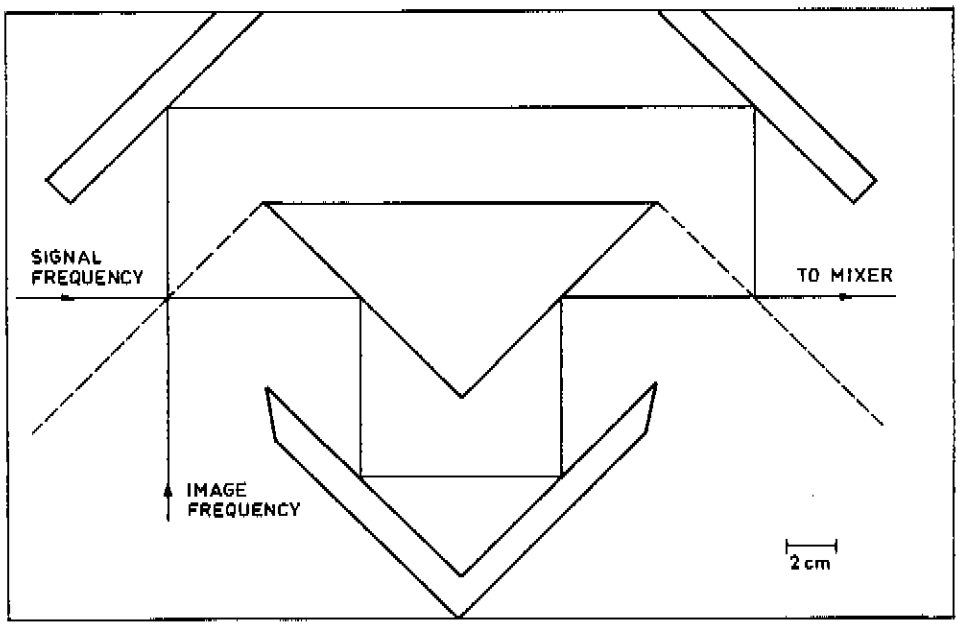

Figure 26b. Single sideband filter.

A dielectric (rexolite) phase modulator at Brewster's angle is used to periodically introduce a 90° phase shift in the beam path to cancel out standing waves in the telescope system. A second ellipsoidal mirror then focuses the beam through a teflon vacuum window (1.8 mm thick) into the feed horn.

This quasi-optical system was designed for use with a corrugated feed horn [9]. The beam of this horn is quite accurately Gaussian with a beamwidth which is nearly frequency independent over the whole waveguide bandwidth. With a corrugated horn the quasi-optical system should be practically lossless. However, at the time of the receiver

tests reported now, no suitable corrugated horn was available and a rectangular horn was used. Due to this, extra losses were introduced, because significant power was lost in sidelobes. When the system was tuned for DSB, frequency dependent losses of 0.35–1.0 dB were measured for the whole quasi-optical system.

3.3.2. Cooled front end

The front end is in a dewar which is cooled by a 2-stage, closed-cycle helium refrigerator with cooling capacities of 3 W at 15 K and 15 W at 80 K. Before cooling, the dewar is vacuum pumped to a pressure of $\sim 10^{-3}$ torr. The feed horn, ring-filter, mixer, dual directional coupler and the first IF amplifier are all mounted on the 15 K stage; the second IF amplifier is mounted on the 80 K stage (Figure 27).

The phase locked LO (a klystron or a klystron at half the desired LO frequency plus a Schottky diode doubler) is coupled by waveguide (gold-plated steel WR-10, 15 cm long) into the adjustable ring-filter. The ring-filter is designed to operate over the whole WR-10 band when the signal and LO frequencies are separated by 4.5–5.0 GHz. Tests revealed, however, that at some LO frequencies a stop-band partly coincided with the IF band. The mixer is followed by the 30 dB dual directional coupler (insertion loss 0.2 dB) providing the opportunity to test IF matching, amplifier gain and noise temperature.

The first and second IF amplifiers are a paramp and FET with 15 dB and 23 dB gain, respectively, at 4.5–5.0 GHz. A noise temperature of 24 K has been measured for the IF system. The IF bandwidth is limited to 375 MHz outside the dewar by a band-pass filter.

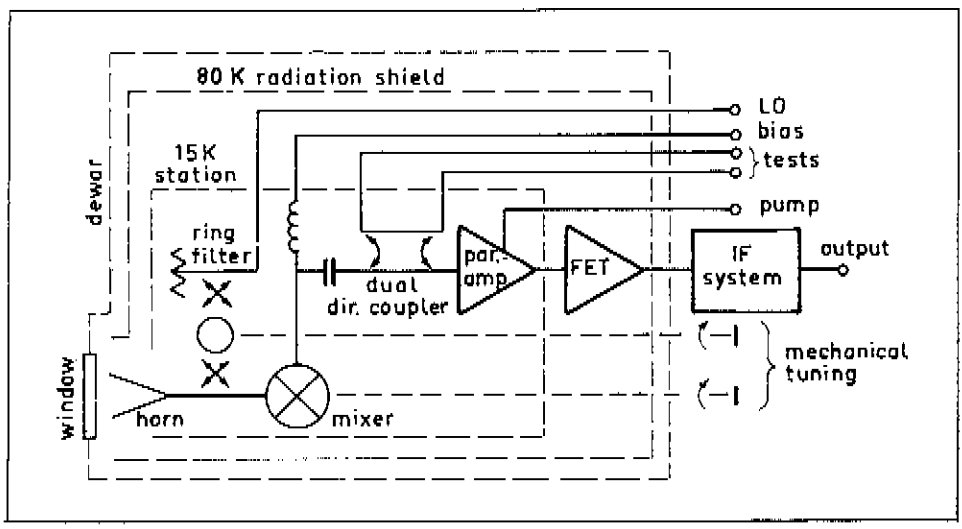

Figure 27. Cooled front end.

3.3.3. Performance of the receiver and the mixer

For the cooled front end noise temperatures of T_{RDSB} = 140 – 230 K have been measured in the laboratory at any local oscillator frequency from 75 to 120 GHz using mixer no. 5 in the receiver. Also, using mixer no. 2, a noise temperature of T_{RDSB} = 140 K has been measured at f_{LO} = 110 GHz. This was realized with an optimum LO

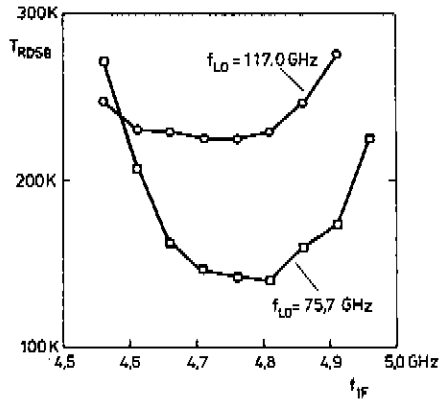

Figure 28. DSB receiver noise temperature versus f_{IF}.

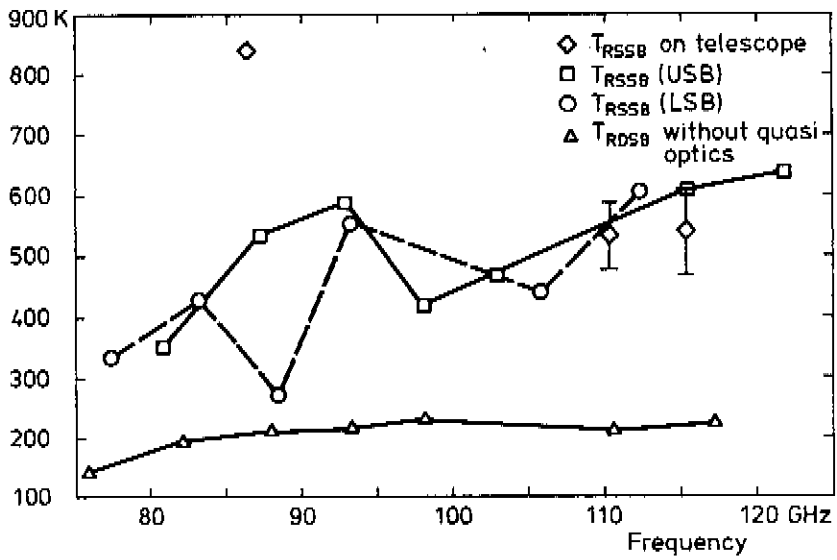

Figure 29. Receiver noise temperature measurement results.

power of 30–50 μW. These results were measured in front of the vacuum window. For the total receiver including the quasi-optics tuned for DSB, T_{RDSB} values were 26 % – 8 % higher at frequencies 75–120 GHz, respectively. This was caused by losses in the quasi-optics due to the sidelobes of the feed horn. Also the sideband ratio L_i/L_s was evaluated at each measurement point and was found to be almost always very close to 0 dB, the only exception was f_{LO} = 82.1 GHz which yielded a ratio of 4.0 dB. Figure 28 shows the variation of the noise temperature T_{RDSB} versus f_{IF} at two local oscillator frequencies. The cooled mixer never requires more LO power than a few hundreds of μW.

The receiver with the quasi-optical SSB filter attached is easily tuned for the best SSB noise temperature by using the sliding backshort. In the laboratory, the best SSB total receiver noise temperature achieved was 275 K at 88 GHz using mixer no. 5. With the same mixer $T_{RSSB} < 600$ K was measured over the frequency range 75–123 GHz. In this mode the sideband ratio L_i/L_s of the mixer was measured to vary from 2 dB to 14 dB at optimum operation points. At many frequencies $T_{RSSB} > 2T_{RDSB}$ despite the suppression of the image in the mixer, even though a 77 K image load was used. This is due to the quasi-optics and ring-filter. Figure 29 summarizes the receiver noise tempera-

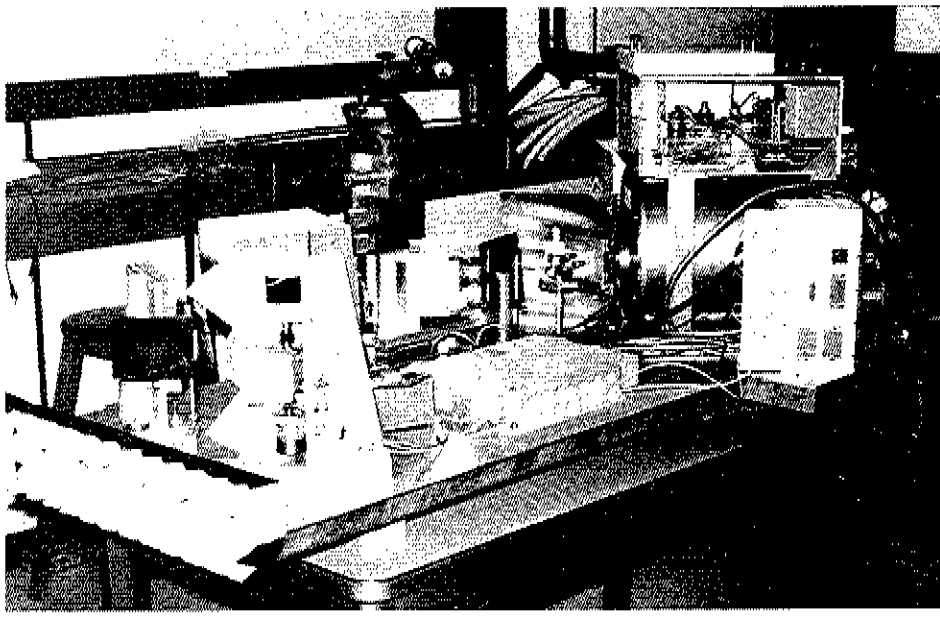

Figure 30. Complete receiver.

ture measurements. The overall measurement accuracy in these measurements is better than ±5 %.

For this mixer the conversion loss remains about at its room temperature value when cooled (i.e. L_C = 6.5–7.0 dB). Neglecting the loss and reflection of the vacuum window, and assuming that the loss of the ring-filter is invariable, the DSB mixer noise temperature can be easily calculated from an equation similar to Equation (18) using T = 15 K instead of T_{room}. This calculation reveals that T_{MDSB} = 60–140 K when f_{LO} = 75–120 GHz. Similarly, for the SSB case, one can calculate T_{MSSB} using equations given in Appendix A and taking the quasi-optics properly into account. At f_s = 88 GHz this calculation gives T_{MSSB} = 90 ± 20 K.

This receiver (Figure 30) has been in continuous operation on the telescope for several months which speaks in favor of the high reliability of the mixer.

4. CONCLUSIONS

In the work reported here both a Josephson point contact mixer for 30–40 GHz and a cooled Schottky diode mixer for 75–120 GHz have been designed and extensively tested. In the design work many methods such as utilization of literature, computer aided design, scaled model studies, cut and try techniques and so on have been used. In measurements the methods used cover a wide range from simple point by point measurements to sophisticated automatic sweep measurements. For example, the very first wide band sweep measurement ever made at frequencies over 200 GHz was carried out in this work.

The Schottky diode mixer developed in this work has several new features: waveguide, backshort, RF filter and IF matching. Without doubt the wide RF range achieved is due to these improved details. The total Schottky mixer receiver described here does not at present reach the best T_{RSSB} values reported at 115 GHz, but it does at 88 GHz with $T_{RSSB} = 275$ K. In addition, its ultra wide range of operation frequencies, 75–120 GHz, with $T_{RDSB} \leqslant 230$ K and $T_{RSSB} \leqslant 500$ K makes it the state-of-the-art receiver. It is very likely that a few changes will improve the receiver performance considerably and result in $T_{RSSB} \leqslant 300$ K over the whole WR-10 band. A new corrugated feed horn will couple better into the quasi-optics. A teflon vacuum window with matching grooves will reduce reflection losses at the edges of the frequency band. Also, the IF matching can be reoptimized to give a wider IF bandwidth. The ring-filter should be changed as well.

The experiment with the Josephson point contact mixer was carried out a few years before the Schottky mixer experiment. The achieved results were modest. This mixer stays far behind the top results in noise performance, although the conversion loss $L_C =$ 5 dB was promising. One should remember, however, that in this experiment no extra cold attenuators were used in front of the mixer to prevent the room temperature noise from saturating the mixer as was the case with the best results reported in the literature. The mechanical stability of this point contact mixer is comparable with the most reliable Josephson point contact mixers reported. Some weak details of this mixer, especially the IF coupling, are readily corrected and, thus, the performance can be easily improved. The remedy which would make it competitive with Schottky mixers is, however, not in sight.

As one can see in the case of the Schottky mixer receiver, the SSB receiver noise temperature is by no means twice the DSB receiver noise temperature as is the common belief. The reason is, first, that the image termination noise contributes considerably to the SSB receiver noise temperature and, second, that at a given frequency the best DSB operation point does not generally coincide with the best SSB operation point. To correct that and other incorrect beliefs and also to correctly relate the noise temperature to the noise figure in different operation modes, the discussion in Appendix A is published together with the experimental work.

REFERENCES

1. BENSON, F.A., STEVEN, D.H., Rectangular-waveguide attenuation at millimeter wavelengths. Proc. IEE **110**(1963)6, p. 1008–1014.

2. BREWER, M.K., RÄISÄNEN, A.V., in preparation, (1980).

3. CARLSON, E.R., SCHNEIDER, M.V., MCMASTER, T.F., Subharmonically pumped millimeterwave mixers. IEEE Trans. Microwave Theory Tech. MTT-**26**(1978)10, p. 706–715.

4. Description of the noise performance of amplifiers and receiving systems. Proc. IEEE **51**(1963)3, p. 436–442.

5. DOLAN, G.J., PHILLIPS, T.G., WOODY, D.P., Low noise 115 GHz mixing in superconducting oxide barrier tunnel junctions. Appl. Phys. Lett. **34**(1979)5, p. 347–349.

6. ERICKSON, N.R., A 0.9 mm heterodyne receiver for astronomical observations. IEEE MTT-S International Microwave Symposium, Ottawa, 1978.

7. ERICKSON, N.R., A 200–300 GHz heterodyne receiver. IEEE MTT-S International Microwave Symposium, Washington D.C., 1980.

8. FRIIS, H.T., Noise figures of radio receivers. Proc. IRE **32**(1944)7, p. 419–422.

9. GOLDSMITH, P.F., in preparation, (1980).

10. HELD, D.N., KERR, A.R., Conversion loss and noise of microwave and millimeterwave mixers: Part 1 – Theory. IEEE Trans. Microwave Theory Tech. MTT-**26**(1978)2, p. 49–55.

11. IRE standards on methods of measuring noise in linear twoports, 1959. Proc. IRE **48**(1960)1, p. 61–68.

12. JOSEPHSON, B.D., Possible new effects in superconductive tunnelling. Phys. Lett. **1**(1962)7, p. 251–252.

13. JOSEPHSON, B.D., Supercurrents through barriers. Adv. in Phys. **14**(1965)56, p. 419–451.

14. KERR, A.R., Low-noise room temperature and cryogenic mixers for 80–120 GHz. IEEE Trans. Microwave Theory Tech. MTT-**23**(1975)10, p. 781–787.

15. KERR, A.R., Shot-noise in resistive-diode mixers and the attenuator noise model. IEEE Trans. Microwave Theory Tech. MTT-**27**(1979)2, p. 135–140.

16. KITTEL, C., Introdcution to solid state physics. New York, John Wiley, 1976.

17. KOLLBERG, E., Schottky barrier diode mixers. URSI Symposium on Millimeter Wave Technology, Grenoble, 1980.

18. LIDHOLM, S., Millimeter-wave mixers for radio astronomy applications in the frequency range 80–120 GHz. Göteborg 1978. Chalmers University of Technology, School of Electrical Engineering, Technical report no. 75.

19. LINKE, R.A., private communication.

20. LINKE, R.A., SCHNEIDER, M.V., CHO, A.Y., Cryogenic millimeter-wave receivers using molecular beam epitaxy diodes. IEEE Trans. Microwave Theory Tech. MTT-26 (1978)12, p. 935–938.

21. MARCUVITZ, N., ed., Waveguide handbook. New York, McGraw-Hill, 1951.

22. MATTHAEI, G.L., YOUNG, L., JONES, E.M.T., Design of microwave filters, impedance-matching networks, and coupling structures. New York, McGraw-Hill, 1964.

23. MCCUMBER, D.E., Effect of ac impedance on dc voltage-current characteristics of superconductor weak link junctions. J. Appl. Phys. **39**(1968)7, p. 3113–3118.

24. MEHARRY, D.E., A millimeter wavelenght transferred electron oscillator. Helsinki 1977. Helsinki University of Technology, Radio Laboratory, Report S 99.

25. NEUMAIER, K., A reliable clean niobium point contact SQUID. Cryogenics **16**(1976)2, p. 117–118.

26. PADOVANI, F.A., STRATTON, R., Field and thermionic-field emission in Schottky barriers. Solid-state electronics **9**(1966), p. 695–707.

27. PHILLIPS, T.G., JEFFERTS, K.B., A low temperature bolometer heterodyne receiver for millimeter wave astronomy. Rev. Sci. Instrum. **44**(1973)8, p. 1009–1014.

28. PIPPARD, A.B., Metallic conduction at high frequencies and low temperatures. Advances in Electronics and Electron Physics **6**(1954), p. 1–45.

29. PREDMORE, R., GOLDSMITH, P., RÄISÄNEN, A., PARRISH, P., MARRERO, J., KOT, R., Low-noise quasi-optical receiver for 75 to 115 GHz. URSI Symposium on Millimeter Wave Technology, Grenoble, 1980.

30. RICHARDS, P.L., SHEN, T-M., Superconductive devices for millimeter wave detection, mixing and amplification. Submitted to IEEE Trans. Electron Devices (1980).

31. RÄISÄNEN, A.V., Experiments with Josephson point-contact mixer at millimeter waves. XXV International Scientific Congress on Electronics, Rome, 1978.

32. RÄISÄNEN, A.V., BREWER, M.K., Design and test of wideband non-contacting millimeter waveguide backshorts. The Fifth International Conference on Infrared and Millimeter Waves, Würzburg, 1980.

33. RÄISÄNEN, A.V., PREDMORE, C.R., PARRISH, P.T., GOLDSMITH, P.F., MARRERO, J.L., KOT, R.A., SCHNEIDER, M.V., A cooled Schottky-diode mixer for 75–120 GHz. 10th European Microwave Conference, Warsaw, 1980.

34. SCHNEIDER, M.V., private communication.

35. SCHNEIDER, M.V., LINKE, R.A., CHO, A.Y., Low-noise millimeter-wave mixer diodes prepared by molecular beam epitaxy (MBE). Appl. Phys. Lett. **31**(1977)3, p. 219–221.

36. SOLLNER, G., private communication.

37. TAUR, Y., CLAASSEN, J.H., RICHARDS, P.L., Josephson junctions as heterodyne detectors. IEEE Trans. Microwave Theory Tech. MTT-22(1974)12, p. 1005–1009.

38. TAUR, Y., KERR, A.R., Low-noise Josephson mixers at 115 GHz using recyclable point contacts. Appl. Phys. Lett. 32(1978)11, p. 775–777.

39. TORREY, H.C., WHITMER, C.A., Crystal rectifiers. New York, McGraw-Hill, 1948.

40. VOWINKEL, B., Heterodynempfänger mit Schottky- und Josephson-Mischer für radioastronomische Beobachtungen im millimeter-Wellenbereich. Ph. D. dissertation, Bonn University, 1978.

41. WEINREB, S., Millimeter-wave varactor down-converters. Workshop on Diode Mixers at Millimeter Wavelengths, Bonn, 1977.

42. WEINREB, S., KERR, A.R., Cryogenic cooling of mixers for millimeter and centimeter wavelengths. IEEE J. Solid-State Circuits SC-8(1973)1, p. 58–63.

43. WRIXON, G.T., Low-noise diodes and mixers for the 1-2-mm wavelength region. IEEE Trans. Microwave Theory Tech. MTT-22(1974)12, p. 1159–1165.

44. WRIXON, G.T., Schottky-diode realization for low-noise mixing at millimeter wavelengths. IEEE Trans. Microwave Theory Tech. MTT-24(1976)11, p. 702–706.

45. ZIMMERMAN, J.E., A review of the properties and applications of superconducting point contacts. Proc. 1972 Appl. Superconductivity Conf., Annapolis, 1972.

APPENDIX A.

FORMULAS FOR THE NOISE TEMPERATURE AND NOISE FIGURE OF MIXER AND A HETERODYNE RECEIVER DERIVED FROM THE BASIC NOISE FIGURE DEFINITION

The noise figure and noise temperature of a mixer are quantities which continuously cause a lot of confusion. The reason for this confusion is the presence of an image in a mixer. The most frequent errors in noise figure and noise temperature usage are made in the following areas:

- The single sideband (SSB) quantities of a broad band mixer are confused with the respective quantities of a narrow band (image rejected) mixer.
- Depending on the situation, the noise generated in the image termination is to be included as part of either mixer noise or source noise.
- Many »rules-of-thumb» used generally by radar engineers in the fifties for calculating SSB quantities from DSB quantities (or vice versa) of a broad band mixer are unfortunately still used.

In this appendix we derive equations for the noise figure and noise temperature of a mixer in different cases of its operation beginning from the basic definition of the noise figure given by FRIIS [8] and IRE [11]. Also, we give suggestions on how to measure these quantities. The generation of noise itself is beyond the scope of this discussion.

A1. Definitions and assumptions

The spectrum associated with a mixer is shown in Figure A1. All harmonic frequencies are assumed to be reactively terminated. The IF port is assumed to be conjugate-matched.

Conventionally we divide mixers into two classes. A broad band mixer (also called: a double sideband mixer or a three frequency mixer) has resistive terminations in both the signal and image band; physically the same or perhaps separated. The conversion losses L_s (the loss from the signal frequency f_s to the intermediate frequency f_{IF}) and L_i (the loss from the image frequency f_i to the intermediate frequency f_{IF}) may be equal or inequal. On the other hand, a narrow band mixer (also called: a single sideband mixer, an image rejection mixer or a two frequency mixer) has a resistive termination only in the signal sideband while the termination in the image sideband seen by the diode is reactive. Now we label the conversion loss from the signal band to the intermediate frequency band as L.

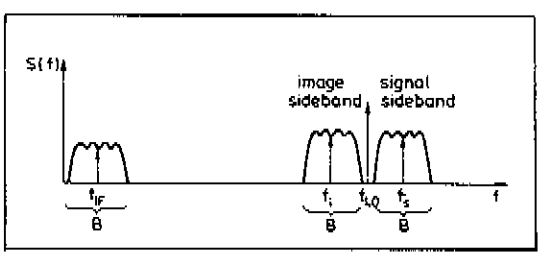

Figure A1. The spectrum associated with a mixer.

In order to better understand the difference between these two mixers at millimeter waves, let us consider an actual millimeter wave mixer. Basically we may have the same device in both cases, but we use it in different ways. First of all we can clearly distinguish two types of operation: (1) a double sideband operation (DSB), when the reception of both signal and image band is useful, for example remote sensing; and (2) a single sideband operation (SSB), when only the signal band input is useful, for example spectral line astronomy. In the DSB case we use a broad band mixer with physically the same signal and image load and a case $L_s \cong L_i$ is desirable but not necessary. In the SSB case we have several possibilities: (a) We use a broad band mixer as before, but now the antenna noise from the image band makes the sensitivity of our receiver worse. (b) We still use a broad band mixer, but we separate the image load and we are able to reduce its physical temperature. Or, (c) we use a narrow band mixer by making the image load seen by the diode reactive by adjusting a movable backshort or inserting a high (or low) -pass filter in front of the mixer. While this makes $L_i \to \infty$ and the image termination noiseless, it also definity changes L_s, so we use a new symbol L instead of L_s.

A2. Noise figure and noise temperature

The noise figure of a linear two-port is defined [11]* by

$$F \equiv \frac{N_{out}}{GN_{in}}, \tag{A 1}$$

where N_{in} is the available noise power in a bandwidth B from a termination at temperature T_0 = 290 K connected to the input of the device, and N_{out} is the total noise power available at the output port in a bandwidth B when the input power is N_{in}. G is the available power gain of the twoport for incoherent signals from an input bandwidth of B to an output bandwidth of B.

The effective input noise temperature or equivalent noise temperature is defined by means of the noise figure as follows:

$$T_e \equiv T_0(F-1) \tag{A 2}$$

or

$$F \equiv 1 + \frac{T_e}{T_0}, \tag{A 3}$$

where T_0 is the absolute reference temperature of 290 K.

A3. Intrinsic noise of a mixer

The mixer diode noise temperature is said to be T_D if the noise power available from the diode equals the noise power from an equivalent resistor at physical temperature T_D. Equivalently, the noise temperature T_D can be understood as the physical temperature of an attenuator which gives the same noise power output as the mixer does when the input terminals of both are connected to a matched termination at T_0.

*Later another definition has been given [4], but it has a special note which neglects the noise from an unused image termination. This note causes, in some cases, a controversy between the definition and measurements as we can see later in this appendix.

By using the latter concept of the diode noise temperature definition, we can calculate the intrinsic noise temperature T_{int} of a mixer referred to the input.

If both the attenuator and its input termination are at temperature T_D the attenuator absorbs and emits the same amount of energy. If we measure the noise output power from this attenuator we will get the result:

$$N_{out} = kBT_D = N_{in}e^{-\tau} + N_{int} = kBT_De^{-\tau} + kBT_D(1 - e^{-\tau}), \tag{A 4}$$

where τ is the optical depth which describes the rate of the absorption and emission in the attenuator. Now, we know that the intrinsic noise power is

$$N_{int} = kBT_D(1 - e^{-\tau}). \tag{A 5}$$

If the temperature of the matched input termination is T_0; the output noise power will be

$$N_{out} = kB[T_0e^{-\tau} + T_D(1 - e^{-\tau})]. \tag{A 6}$$

Using the symbol L instead of e^{τ}, we obtain

$$N_{out} = kB\left[\frac{T_0}{L} + T_D\left(1 - \frac{1}{L}\right)\right] = kB\left[\frac{T_0}{L} + \frac{T_{int}}{L}\right]. \tag{A 7}$$

If a narrow band mixer and its input termination are in thermal equilibrium we get exactly the same equation as (A 4) for the output noise power. When a frequency conversion takes place and L describes the conversion loss we conclude that Equations (A 6) and (A 7) are also valid. Accordingly, for a narrow band mixer,

$$T_{int} = T_D(L - 1). \tag{A 8}$$

Let us then consider a multiport multifrequency circuit in which there are N input frequencies (all bandwidths are B) all having resistive terminations. If we measure the output noise power at the output frequency (bandwidth B) when the whole circuit is at the temperature T_D the result will be:

$$N_{out} = kBT_D = \sum_{n=1}^{N} N_{in,n}\frac{1}{L_n} + N_{int} = kBT_D\sum_{n=1}^{N}\frac{1}{L_n} + kBT_D\left(1 - \sum_{n=1}^{N}\frac{1}{L_n}\right), \tag{A 9}$$

where L_n is the loss from the nth input port to the output port. Allowing the nth matched input termination to be at a temperature T_n, we obtain the final result:

$$N_{out} = kB\left[\sum_{n=1}^{N}\frac{T_n}{L_n} + T_D\left(1 - \sum_{n=1}^{N}\frac{1}{L_n}\right)\right]. \tag{A10}$$

In the case of a broad band mixer ($N = 2$, Figure A2) with both input terminations at T_0 we get

$$N_{out} = kB\left[\frac{T_0}{L_s} + \frac{T_0}{L_i} + \left(1 - \frac{1}{L_s} - \frac{1}{L_i}\right)T_D\right] = kB\left[\frac{T_0}{L_{DSB}} + \left(1 - \frac{1}{L_{DSB}}\right)T_D\right] \tag{A11}$$

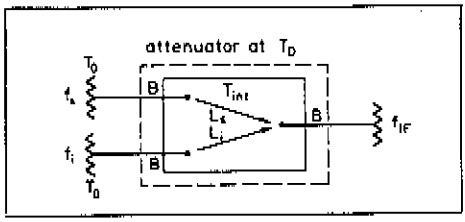

Figure A2. A mixer as an attenuator.

or equivalently

$$N_{out} = kB\left[\frac{T_0}{L_s} + \frac{T_0}{L_i} + \frac{T_{int}}{L_s} + \frac{T_{int}}{L_i}\right] = kB\left[\frac{T_0}{L_{DSB}} + \frac{T_{int}}{L_{DSB}}\right], \tag{A12}$$

which together give

$$T_{int} = T_D\left(\frac{L_s L_i}{L_s + L_i} - 1\right) = T_D(L_{DSB} - 1). \tag{A13}$$

In the intrinsic noise temperature calculations above the conversion loss is assumed to be determined exclusively by the mixing element (diode). I.e., the transmission line losses in the mixer are neglected, because their small noise contribution depend on the ambient temperature and not on T_D.

A4. Noise figure and noise temperature of a mixer

The simple presentation of a mixer in Figure A3 helps to give the quantities needed in noise figure calculations.

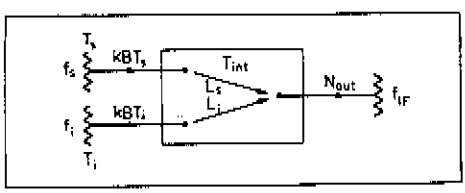

Figure A3. A simple model for a mixer.

A4.1. A narrow band mixer

In this case $L_i \to \infty$ and $L_s \to L$.

$$N_{in} = kBT_s \tag{A14}$$

$$N_{out} = \frac{kB}{L}(T_s + T_{int}) \tag{A15}$$

$$G = \frac{1}{L} \tag{A16}$$

Using the noise figure definition (A1) and requiring $T_s = T_0$, we obtain

$$F_M = 1 + \frac{T_M}{T_0} \equiv \frac{N_{out}}{GN_{in}} = \frac{\frac{kB}{L}(T_0 + T_{int})}{\frac{1}{L}kBT_0} = 1 + \frac{T_{int}}{T_0}, \tag{A17}$$

where we have labelled the noise figure and equivalent noise temperature of a narrow band mixer as F_M and T_M respectively.

By combining (A8) and (A17), we get

$$T_M = T_{int} = T_D(L - 1) . \tag{A18}$$

A4.2. A broad band mixer

(1) DSB operation

Both the signal and image terminations are physically the same ($T_i = T_s$).

$$N_{in} = kBT_s \tag{A19}$$

$$N_{out} = \frac{kB}{L_{DSB}} (T_s + T_{int}) \tag{A20}$$

$$G = \frac{1}{L_i} + \frac{1}{L_s} = \frac{1}{L_{DSB}} . \tag{A21}$$

When substituting these into the noise figure definition, we again require $T_s = T_0$.

$$F_{MDSB} \equiv 1 + \frac{T_{MDSB}}{T_0} \equiv \frac{N_{out}}{GN_{in}} = \frac{\frac{kB}{L_{DSB}} (T_0 + T_{int})}{\frac{1}{L_{DSB}} kBT_0} = 1 + \frac{T_{int}}{T_0} . \tag{A22}$$

Now we can solve for the equivalent noise temperature of a broad band mixer in a DSB operation T_{MDSB}. Recalling (A13),

$$T_{MDSB} = T_{int} = T_D(L_{DSB} - 1) . \tag{A23}$$

(2) SSB operation

In this case signal and image terminations can be physically the same or separated ones (both resistive).

$$N_{in} = kBT_s \tag{A24}$$

$$N_{out} = \frac{kB}{L_s}(T_s + T_{int}) + \frac{kB}{L_i}(T_i + T_{int}) \tag{A25}$$

$$G = \frac{1}{L_s} . \tag{A26}$$

Again, by definition, $T_s = T_0$ so

$$F_{MSSB} \equiv 1 + \frac{T_{MSSB}}{T_0} \equiv \frac{N_{out}}{GN_{in}} = \frac{\frac{kB}{L_s}(T_0 + T_{int}) + \frac{kB}{L_i}(T_i + T_{int})}{\frac{1}{L_s} kBT_0}$$

$$= 1 + \frac{\left(1 + \frac{L_s}{L_i}\right)T_{int} + \frac{L_s}{L_i} T_i}{T_0} . \qquad (A27)$$

From (A13) and (A27) we obtain the equivalent noise temperature of a broad band mixer in the SSB operation T_{MSSB}:

$$T_{MSSB} = \left(1 + \frac{L_s}{L_i}\right)T_{int} + \frac{L_s}{L_i} T_i = T_D\left(L_s - 1 - \frac{L_s}{L_i}\right) + \frac{L_s}{L_i} T_i . \qquad (A28)$$

In this case we get the result that the noise from the unused image termination is to be included to the mixer equivalent noise temperature. Also, common sense speaks in favor of this fact because the signal and image termination are now separable. Thus the receiver can be built so that the diode sees a low noise (cooled) resistive termination at the image frequency while the operation of the mixer otherwise remains the same.

One possible physical realization of the receiver suggested above is shown in Figure A4. Another possible realization of this receiver is the use of a quasi-optical diplexer in front of the feed horn.

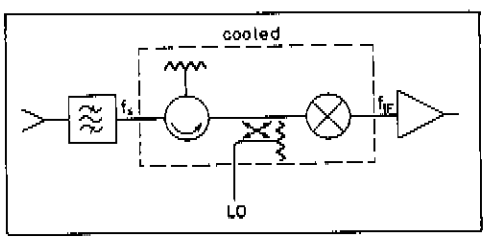

Figure A4. A broad band mixer having a separate cooled termination at the image frequency.

A4.3. Derivations of some often used »rules-of-thumb» concerning a broad band mixer

(1) Let us consider the situation when $L_s = L_i$ and $T_i = 0$, which may be a desired condition in SSB operation.

Substituting these values into Equations (A23) and (A28) we obtain

$$T_{MDSB} = T_{int} \qquad (A29)$$

$$T_{MSSB} = 2T_{int} . \qquad (A30)$$

These together give the well known formula

$$T_{MDSB} = 1/2 T_{MSSB} . \qquad (A31)$$

Further, substituting (A31) into definitions (A22) and (A27), we get another well known formula

$$F_{MDSB} = 1/2(F_{MSSB} + 1) . \quad (A32)$$

(2) Let us now consider another case, where $L_i = L_s$ and $T_i = T_0$.
By substituting $L_i = L_s$ and $T_i = T_0$ into Equations (A23) and (A28) we obtain

$$T_{MDSB} = T_{int} \quad (A33)$$

$$T_{MSSB} = 2T_{int} + T_0 , \quad (A34)$$

which together give

$$T_{MDSB} = 1/2(T_{MSSB} - T_0) . \quad (A35)$$

Finally, substituting (A35) into definitions (A22) and (A27) we get

$$F_{MDSB} = 1/2F_{MSSB} . \quad (A36)$$

(3) We cannot derive any connection formulas between the broad band mixer noise quantities and the narrow band mixer noise quantities. Not even in the case when the narrow band receiver is built by putting a high-pass filter in front of a broad band mixer, because without a new measurement we do not know how L_s is going to change.

A5. The receiver noise temperature and the system noise temperature

In the following we calculate the system noise temperature and the receiver noise temperature in every case of the mixer's operation by using the equations derived above. The following calculations are based on the facts (Figure A5):

$$T_{system} = T_{antenna} + T_{receiver} \quad (A37)$$

$$N_{out} = T_{system} \frac{G_{IF}}{L_{total}} kB . \quad (A38)$$

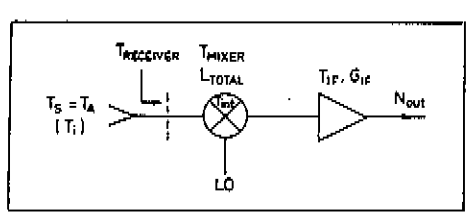

Figure A5. A mixer receiver.

In the case of *a narrow band mixer* $T_{mixer} = T_M = T_{int}$ and $L_{total} = L$. Then we have

$$\frac{1}{kB} N_{out} = T_A \frac{G_{IF}}{L} + T_{int} \frac{G_{IF}}{L} + T_{IF} G_{IF} = (T_A + T_{int} + LT_{IF}) \frac{G_{IF}}{L} , \quad (A39)$$

from which it follows that

$$T_R = T_{int} + LT_{IF} = T_M + LT_{IF} \quad (A40)$$

$$T_{sys} = T_A + T_M + LT_{IF} \,. \tag{A41}$$

For *a broad band mixer* we have to consider two different cases:

(1) DSB operation.

Now we have $T_{mixer} = T_{MDSB} = T_{int}$, $L_{total} = L_{DSB}$ and $T_i = T_A$.

$$\frac{1}{kB} N_{out} = T_A \frac{G_{IF}}{L_s} + T_A \frac{G_{IF}}{L_i} + T_{int} \frac{G_{IF}}{L_{DSB}} + T_{IF} G_{IF}$$

$$= (T_A + T_{int} + L_{DSB} T_{IF}) \frac{G_{IF}}{L_{DSB}} \,, \tag{A42}$$

from which we obtain

$$T_{RDSB} = T_{int} + L_{DSB} T_{IF} = T_{MDSB} + L_{DSB} T_{IF} \tag{A43}$$

$$T_{sys,DSB} = T_A + T_{MDSB} + L_{DSB} T_{IF} \,. \tag{A44}$$

(2) SSB operation (the signal and image loads may be physically separated).

In this case we have $T_{mixer} = T_{MSSB} = \left(1 + \frac{L_s}{L_i}\right) T_{int} + \frac{L_s}{L_i} T_i$ and $L_{total} = L_s$.

$$\frac{1}{kB} N_{out} = \frac{T_A}{L_s} G_{IF} + \frac{T_i}{L_i} G_{IF} + T_{int} \frac{G_{IF}}{L_{DSB}} + T_{IF} G_{IF}$$

$$= \left[T_A + \frac{L_s}{L_i} T_i + \left(1 + \frac{L_s}{L_i}\right) T_{int} + L_s T_{IF} \right] \frac{G_{IF}}{L_s} \,, \tag{A45}$$

which gives

$$T_{RSSB} = \left(1 + \frac{L_s}{L_i}\right) T_{int} + \frac{L_s}{L_i} T_i + L_s T_{IF} = T_{MSSB} + L_s T_{IF} \tag{A46}$$

$$T_{sys,SSB} = T_A + T_{MSSB} + L_s T_{IF} \,. \tag{A47}$$

As we have seen, in every case above it follows that Equation (A37) and the equation

$$T_{receiver} = T_{mixer} + T_{total} T_{IF} \tag{A48}$$

are in harmony. This fact again speaks in favor of the statement that the noise from an unused image termination is to be included in the mixer noise.

A6. Noise measurements

Let us consider the well known *Y*-factor method where a hot (room temperature, T_H = 295 K) and a cold (liquid nitrogen, T_C = 77 K) load are used.

A6.1. A narrow band mixer

When the hot and cold load are placed in front of the feed the following noise powers can be measured at the intermediate frequency. Respectively,

$$N_H = (T_H + T_R)kBG_{IF}\frac{1}{L} = (T_H + T_M + LT_{IF})kBG_{IF}\frac{1}{L} \tag{A49}$$

$$N_C = (T_C + T_R)kBG_{IF}\frac{1}{L} = (T_C + T_M + LT_{IF})kBG_{IF}\frac{1}{L}\ . \tag{A50}$$

Now

$$Y \equiv \frac{N_H}{N_C} = \frac{T_H + T_R}{T_C + T_R} = \frac{T_H + T_M + LT_{IF}}{T_C + T_M + LT_{IF}}\ , \tag{A51}$$

from which we can solve

$$T_R = T_M + LT_{IF} = \frac{T_H - YT_C}{Y - 1}\ . \tag{A52}$$

If we want to know T_M another hot-cold load measurement is needed for the intermediate frequency amplifier from which we get T_{IF}. Let us write

$$N_{H,IF} = (T_H + T_{IF})kBG_{IF} \tag{A53}$$

and

$$N_{C,IF} = (T_C + T_{IF})kBG_{IF} \tag{A54}$$

as the measured noise powers when a room temperature load and a cold load, respectively, are connected to the input of the IF amplifier. Now we are able to solve for L:

$$L = \frac{N_{H,IF} - N_{C,IF}}{N_H - N_C} \tag{A55}$$

and then T_M can be solved for from (A52).

A6.2. A broad band mixer with separated signal and image loads

Again we measure noise powers N_H and N_C (see (A45) and (A46)):

$$N_H = (T_H + T_{RSSB})kBG_{IF}\frac{1}{L_s} = (T_H + T_{MSSB} + L_sT_{IF})kBG_{IF}\frac{1}{L_s} \tag{A56}$$

$$N_C = (T_C + T_{RSSB})kBG_{IF}\frac{1}{L_s} = (T_C + T_{MSSB} + L_sT_{IF})kBG_{IF}\frac{1}{L_s}\ , \tag{A57}$$

from which

$$Y \equiv \frac{N_H}{N_C} = \frac{T_H + T_{RSSB}}{T_C + T_{RSSB}} = \frac{T_H + T_{MSSB} + L_sT_{IF}}{T_C + T_{MSSB} + L_sT_{IF}}\ . \tag{A58}$$

And, as before, we obtain the solution (remember that T_{RSSB} and T_{MSSB} now include the noise from the unused image termination)

$$T_{RSSB} = T_{MSSB} + L_s T_{IF} = \frac{T_H - YT_C}{Y - 1} . \tag{A59}$$

In order to solve for T_{MSSB} and L_s also, we continue exactly in the same way as in section A6.1. But, if we are interested in knowing what T_{RDSB} and T_{MDSB} are, it is better to remove the separation of the image and signal terminations and to measure the whole receiver again using the method presented next.

A6.3. A broad band mixer with physically the same load at the signal and image frequencies

Now we measure the Y-factor as follows (see (A42) and (A43)):

$$N_H = (T_H + T_{RDSB})kBG_{IF}\frac{1}{L_{DSB}} = (T_H + T_{MDSB} + L_{DSB}T_{IF})kBG_{IF}\frac{1}{L_{DSB}} \tag{A60}$$

$$N_C = (T_C + T_{RDSB})kBG_{IF}\frac{1}{L_{DSB}} = (T_C + T_{MDSB} + L_{DSB}T_{IF})kBG_{IF}\frac{1}{L_{DSB}} \tag{A61}$$

$$Y \equiv \frac{N_H}{N_C} = \frac{T_H + T_{RDSB}}{T_C + T_{RDSB}} = \frac{T_H + T_{MDSB} + L_{DSB}T_{IF}}{T_C + T_{MDSB} + L_{DSB}T_{IF}} . \tag{A62}$$

T_{RDSB} is solved for easily

$$T_{RDSB} = T_{MDSB} + L_{DSB}T_{IF} = \frac{T_H - YT_C}{Y - 1} . \tag{A63}$$

In order to solve for T_{MDSB} we have to measure T_{IF} and L_{DSB} as before (see (A55)).

If T_{RSSB} and T_{MSSB} are also to be determined we must know T_i (the antenna temperature at the image frequency) under operating conditions. Furthermore, we must measure the ratio L_s/L_i (using a quasioptical filter or coherent signals). Then by using (A43) and (A46) we can solve

$$T_{RSSB} = \left(1 + \frac{L_s}{L_i}\right)T_{RDSB} + \frac{L_s}{L_i}T_i \tag{A64}$$

$$T_{MSSB} = \left(1 + \frac{L_s}{L_i}\right)T_{MDSB} + \frac{L_s}{L_i}T_i . \tag{A65}$$

As we have seen, the measurement of T_R, T_{RSSB} and T_{RDSB} in cases A6.1., A6.2. and A6.3., respectively, is quite easy regardless of the mechanical structure of the receiver. The measurement of other noise quantities, however, may be extremely difficult if the receiver (both the mixer and IF amplifier) is, for example, cooled, because the access to the input of the IF amplifier is then limited.

A7. Concluding remarks

We have derived a consistent (with each other and with measurements) set of equations for noise quantities of heterodyne receivers. Most of these equations, perhaps all, have been published in the literature in separated articles and by different authors, for example [3], [15], [40], but never before, in so far as we know, in a single paper.

Our results definitely say that the noise from an unused image termination of a broad band mixer belongs in the mixer noise. This can also be said: the actual mixer is not only the little box which may have a label MIXER, but the mixer concept must be extended to the input load which may ultimately define the mixer's performance.

As a final conclusion and for comparison, we give the derived noise temperature and noise figure equations of a broad band mixer (or receiver) in the same form of presentation as CARLSON et al. recently presented their equations [3] (Figure A6).

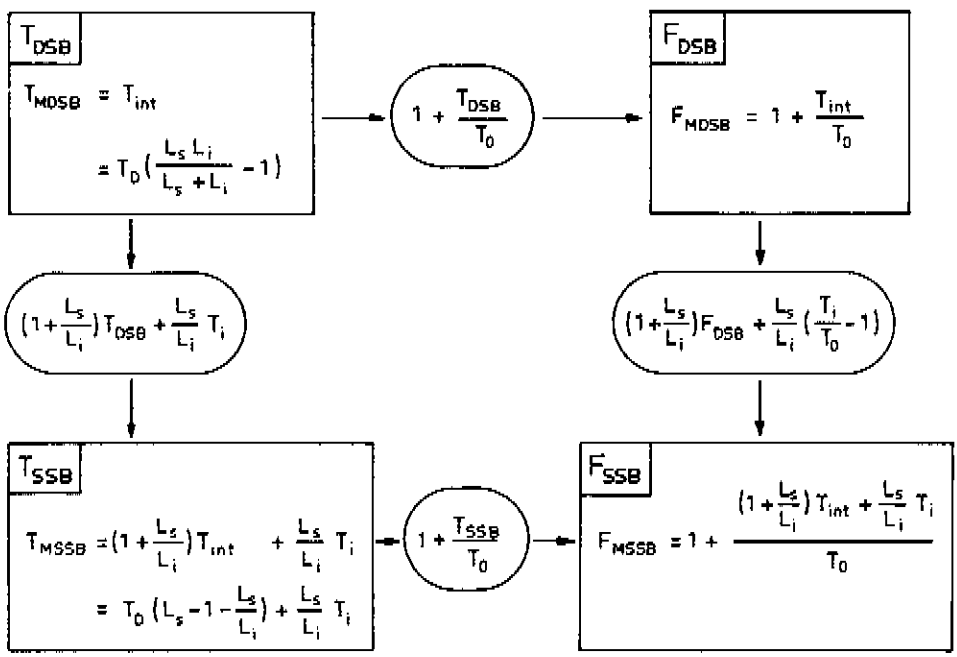

Figure A6. Noise relationships* in receivers which use a broad band mixer. (When compared with the Figure 9 in Reference [3] it will be found that those equations are a special case of the set of equations presented here. In Reference [3] the image temperature T_i is neglected in the expressions for T, but it is assumed to be $T_i = T_0$ in the expressions for F.)

* Both this paper and Reference [3] conflict with Reference [4].

ACTA POLYTECHNICA SCANDINAVICA

Electrical Engineering Series

EI 25 KOHONEN, TEUVO, *A class of randomly organized associative memories.* Helsinki 1971. 19 pp. Sw.kr. 10.00. UDC 621.391

EI 26 HENTINEN, V., *A channel state feedback communication system.* Helsinki 1971. 43 pp. Sw.kr. 10.00. UDC 621.391

EI 27 SOMERVUO, P. and SIRKEINEN, Y., *On the phase stability of parametric amplifiers.* Helsinki 1971. 24 pp. Sw.kr. 10.00. UDC 621.375.7

EI 28 MARIN, LENNART, *Analysis of a slotted circular waveguide.* Stockholm 1971. 23 pp. Sw.kr. 10.00. ISBN 91 7082 025 2. UDC 621.372.823

EI 29 KOHONEN, TEUVO, *Introduction of the principle of virtual images in associative memories.* Helsinki 1971. 15 pp. Sw.kr. 10.00. UDC 621.391

EI 30 VALTONEN, MARTTI, *A new synthesis method for branch-guide directional couplers.* Helsinki 1972. 19 pp. Fmk 8.00. ISBN 951–666–004–5. UDC 538.3:621.3.029.64 621.3.09

EI 31 LINDELL, ISMO V., *Wave normal and ray propagation in lossless positive bianisotropic media.* Helsinki 1972. 22 pp. Fmk 8.00. ISBN 951–666–008–8. UDC 621.372.018.7:517.9

EI 32 JOKINEN, TAPANI, *Utilization of harmonics for self-excitation of a synchronous generator by placing an auxiliary winding in the rotor.* Helsinki 1973. 82 pp. Fmk 8.00. ISBN 951–666–024–X. UDC 621.313.322:538.24:62-56

EI 33 SÄYNÄJÄKANGAS, SEPPO, *A non-destructive electromagnetic method for structural studies of ferrous alloys.* Helsinki 1973. 58 pp. Fmk 8.00. ISBN 951–666–025–8. UDC 669.15:620.179.14

EI 34 LAPPALAINEN, PENTTI, *On the conversion of digital pattern information into raster scan format using hardware implementation.* Helsinki 1974. 74 pp. Fmk 8.00. ISBN 951–666–039–8. UDC 681.323:621.397:513.5

EI 35 HAIKONEN, TERHO, *On multiple scattering by small particles in open resonators.* Helsinki 1975. 31 pp. Fmk 8.00. ISBN 951–666–052–5. UDC 621.372.8:621.3.091

EI 36 MORATH, ERIK, *Magnetic field in the air-gap and load losses in the solid pole surfaces of synchronous machines.* Helsinki 1975. 72 pp. ISBN 951–666–055–X. UDC 621.3.017:621.313.32

EI 37 VALTONEN, MARTTI, *Synthesis of lossless networks consisting of cascaded commensurate transmission lines and frequency-invariant two-ports.* Helsinki 1975. 64 pp. ISBN 951–666–058–4. UDC 621.372.001.1:621.3.049

EI 38 MEHARRY, DAVID, *A theoretical and experimental study of quenched domain oscillations in a transferred electron device.* Helsinki 1976. 64 pp. ISBN 951–666–068–1. UDC 621.372:537.311.33 621.382.001.5

EI 39 MALMIVUO, JAAKKO, *On the detection of the magnetic heart vector – An application of the reciprocity theorem.* Helsinki 1976. 112 pp. ISBN 951–666–071–1. UDC 621.318.38:616.12–073 53.082.78

EI 40 SOMERVUO, PEKKA, *Parametric amplification using a point contact Josephson junction.* Helsinki 1976. 34 pp. ISBN 951–666–077–0. UDC 537.312.62:621.375.7

EI 41 HALTSONEN, SEPPO, *Comparison of logic function realization methods.* Helsinki 1977. 22 pp. ISBN 951–666–095–9. UDC 621.3.049.77:681.325.65:517.1

EI 42 HÄMEENAHO, VEIKKO and LAPPALAINEN, PENTTI, *An analogue image processing system using television camera and monitor with multiple frame interlacing.* Helsinki 1978. 48 pp. ISBN 951–666–108–4. UDC 621.397.3:776.7 655.3.027

ISBN 951–666–127–0
ISSN 0001–6845